Improved airborne scalar gravimetry for regional gravity field mapping and geoid determination

by

Arne Vestergaard Olesen

National Survey and Cadastre – Denmark (KMS)
Rentemestervej 8,
DK-2400 Copenhagen NV
Phone/fax +45 3587 5243/+45 3587 5052
E-mail: avo@kms.dk
http://research.kms.dk/~avo

The present text was together with seven appended papers submitted in July 2002 to the Faculty of Science, University of Copenhagen as a dissertation in partial fulfillment of the requirements for the Ph.D. degree.

Improved airborne scalar gravimetry for regional gravity field mapping and geoid determination

By Arne Vestergaard Olesen

First edition, October 2003

ISBN 87-7866-383-0

ISSN 0908-2867

Abstract

Airborne gravimetry has during the last decade become a really operational way to map the Earths gravity field, mainly because of improvements in GPS technology. Improved inertial sensors have been employed for airborne gravity recovery during the last few years and show some promising results, but the far biggest volume of airborne gravity mapping are done with spring type gravimeters mounted on stabilized platforms, even this sensor technology is quite old. This paper addresses possible improvements in the processing of airborne gravimetry from such a spring type gravimeter system.

One of the biggest advantages of the spring type gravimeter compared to inertial sensors is its superior long-term stability. A new algorithm to correct for platform off-leveling errors is derived and it is shown that this new algorithm in combination with the good drift characteristic for the spring type gravimeter yields virtual bias free data. This is an important point when it comes to geodetic use of the acquired data. The near bias free nature of the data from our system is underlined by the fact that no crossover adjustment procedures are involved in the data reduction.

Also routines to identify and correct for some GPS related errors are outlined. Unfiltered gravity estimates have proven to be a good tool to identify artifact accelerations coming from GPS ambiguity fixing problems, especially under smooth flight conditions.

The resolution of the airborne gravity system is optimized through an analysis of the vertical sensor response. Concepts as apparent K-factor and filter-optimized K-factor are introduced in order to access the combined response of the gravimeter beam and the GPS positioning system.

It is shown that the analyzed system maps gravity with an accuracy of 1.3 mgal at 6 km resolution. This performance may degrade during periods with air turbulence. The noise estimates for four consecutive years of airborne measurements in Greenland ranged from 1.3 to 2.0 mgal. It should be noticed that 6 km is a conservative estimate for the resolution. The filter can under low-turbulent conditions be shortened considerably and still yield virtual the same data accuracy.

Table of content

Introduction

The ability to measure gravity from an aircraft has long been a dream for many geoscientists in order to get a cost-effective and high-resolution gravity-mapping tool, with the potential to cover areas difficult to access by traditional methods. Several airborne gravity systems have been tested and operated during the last 5 decades, but it was not until the Global Positioning System (GPS) matured and could provide a 24 hours worldwide coverage, that airborne measurements became a really operational way to map gravity.

Recent developments in GPS techniques have also boosted the demand for good gravimetric geoid models, the link between traditional heights above sea level and the ellipsoidal height system used in GPS. Thus, improvements in the Global Positioning System have both made airborne gravimetry operational and triggered the interest for the products derived from it. This is the background for National Survey and Cadastre – Denmark (KMS) to undertake airborne gravity surveys since 1996. It has been the author's main task to establish a sound way to process the data from these campaigns and the present text gives a review of my efforts.

There are two main challenges in the processing of airborne gravity data; the first is to separate gravitational accelerations from kinematic aircraft accelerations; this will mainly impact the resolution of the system. A proper separation of gravitational and kinematic accelerations requires a good description of the gravity sensor response. The sensor modeling presented in the following appears to exploit most of the potential of the gravity sensor we use, a LaCoste & Romberg air/marine gravimeter. GPS related errors will also affect the separation of accelerations and routines to identify and model such errors are described as well.

The other challenge in airborne gravity processing is to keep track of the orientation of the sensors during the flight, as this is crucial for the recovery of the longer wavelengths of the gravity field, and hence for geodetic use of the data. A new algorithm for airborne gravity processing that addresses the misalignment or off-level problem is derived and it is shown that this new approach yield virtual bias free data. The near bias free nature of the data from our system is underlined by the fact that no crossover adjustment procedures are involved in the data reduction.

The volume of data analyzed as part of this work represents more than 600 flight hours or approximately 150,000 km. The data are acquired under very diverse climatic and

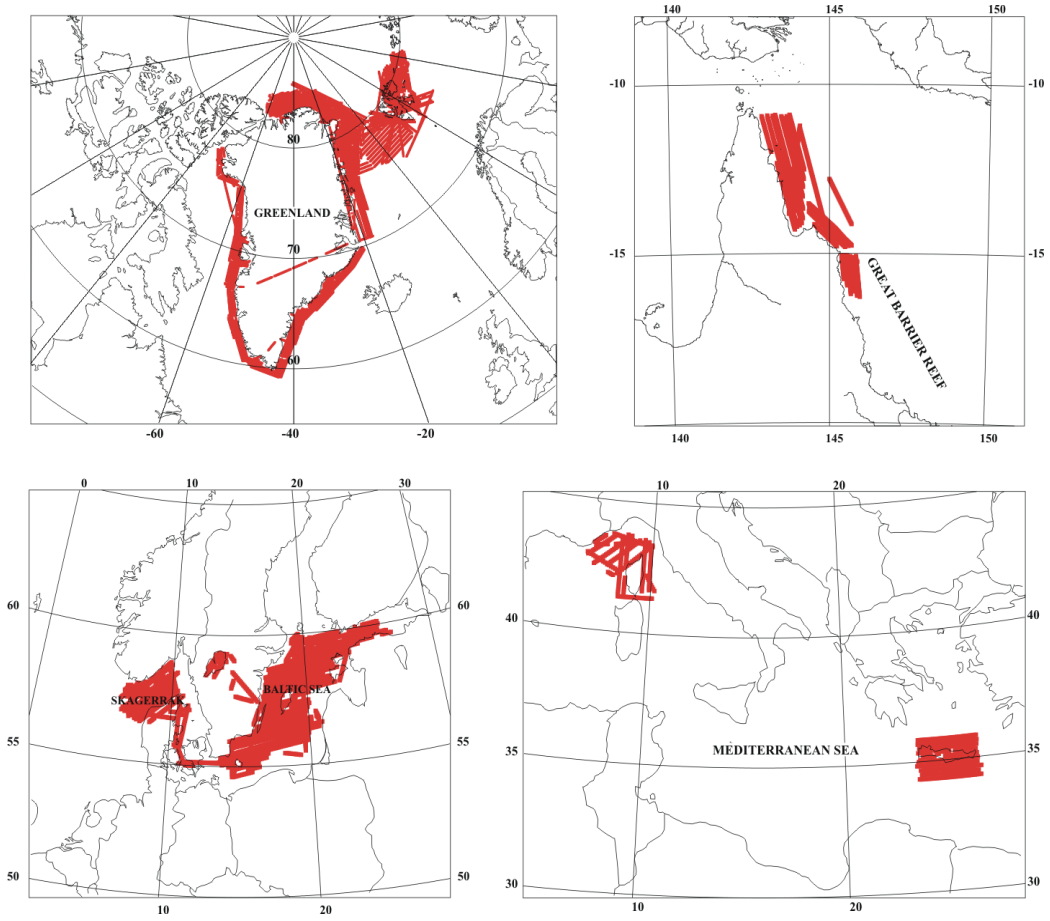

Figure 1. The surveys: Skagerrak 1996. Greenland/Svalbard 1998, 1999, 2000 and 2001. Baltic Sea 1999. Great Barrier Reef 1999. Crete and Corsica 2001. The plots are not on a common scale.

operational conditions, from near the North Pole to near the Equator, see Figure 1, and the analysis presented here therefore give a picture of the system performance for a wide range of circumstances. It is shown that the system yields data accurate to 2 mgal or better when filtered at a resolution of 6 km.

It should be emphasized that this 2 mgal/6 km or better performance is obtained for a wide selection of flight conditions. If we focus on subsets of the data obtained under more favorable conditions, for example the Baltic Sea survey or the Greenland 1998 survey, an accuracy of 1.3 mgal was obtained.

The following text is divided into 3 chapters. The basic theory related to airborne gravity processing is presented in chapter 1. Chapter 2 comprises description of the actual system, sensor modeling and identification of error sources. Survey descriptions are referred to chapter 3. The accuracy of the obtained data is also evaluated in this chapter.

1 Gravity measurements from a vehicle

The basic theory in terms of reference frames and navigation equations is briefly presented in this chapter. Both strapdown and stabilized platform gravity systems are described, with focus on the latter. Detailed equations for the reduction of airborne measurements are given and a new algorithm to correct for platform misalignment errors is formulated.

1.1 Reference frames, navigation equations and gravity

Several coordinate systems or frames are in play in the reduction of gravity measurements from a moving platform. First of all is the inertial frame or i-frame where Newton's laws apply. Next is the Earth-centered-Earth-fixed frame, the e-frame, a Cartesian coordinate system with its origin in the Earth's center of mass and following the rotation of the Earth. The navigation frame, or the n-frame, is closely related to the definition of ellipsoidal coordinates. It is a Cartesian local level system, with origin either on the ellipsoid or at the vehicle. One axis is aligned with the local ellipsoidal normal and the other two axes point north and east. More conventions for the orientation of axis are in use. The one adapted in this context is: East, North, Up. Finally the body frame, which is related to the vehicle, and which is used to describe the installation of the instruments. For details on the reference frames and the transformations among them see e.g. Jekeli (2001).

The transformation from one frame to another is accomplished by a rotation eventually in combination with a simple translation. The rotation $\mathbf{R}_{\mathbf{e}}^{\mathbf{i}}$ from the e-frame to the i-frame is given in matrix form as:

$$\mathbf{R}_{\mathbf{e}}^{\mathbf{i}} = \begin{bmatrix} \cos\omega_{ie}t & -\sin\omega_{ie}t & 0 \\ \sin\omega_{ie}t & \cos\omega_{ie}t & 0 \\ 0 & 0 & 1 \end{bmatrix} \tag{1.1}$$

where t is time and ω_{ie} is the earth rotation rate relative to the inertial frame as measured in the e-frame. The rotation from the e-frame to the n-frame is:

$$\mathbf{R}_{\mathbf{e}}^{\mathbf{n}} = \begin{bmatrix} -\sin\lambda & \cos\lambda & 0 \\ -\sin\varphi\cos\lambda & -\sin\varphi\sin\lambda & \cos\varphi \\ \cos\varphi\cos\lambda & \cos\varphi\sin\lambda & \sin\varphi \end{bmatrix} \tag{1.2}$$

The rotation rates related to (1.1) and (1.2) are given in the navigation frame as:

$$\mathbf{\Omega}_{ie}^{n} = \begin{bmatrix} 0 & -\omega_{ie}\sin\varphi & \omega_{ie}\cos\varphi \\ \omega_{ie}\sin\varphi & 0 & 0 \\ \omega_{ie}\cos\varphi & 0 & 0 \end{bmatrix} \tag{1.3}$$

and

$$\mathbf{\Omega}_{en}^{n} = \begin{bmatrix} 0 & -\dot{\lambda}\sin\varphi & \dot{\lambda}\cos\varphi \\ \dot{\lambda}\sin\varphi & 0 & \dot{\varphi} \\ \dot{\lambda}\cos\varphi & -\dot{\varphi} & 0 \end{bmatrix} \tag{1.4}$$

Newton's Second Law states that the acceleration of a mass is proportional to the sum of the forces acting on it. In the inertial frame this may be written as:

$$\mathbf{a}^{i} = \ddot{\mathbf{r}}^{i} = \bar{\mathbf{g}}^{i} + \mathbf{f}^{i} \tag{1.5}$$

Here $\bar{\mathbf{g}}$ denotes gravitational attraction (the notation $\mathbf{g}$ will be reserved for the gravity vector), $\mathbf{f}$ is the specific force (force per unit mass) and the superscript indicates the reference frame. Projected onto the axis of the n-frame the equation becomes (it should be noted that the relation $\mathbf{a} = \ddot{\mathbf{r}}$ only holds in the i-frame):

$$\begin{aligned} \mathbf{a}^{n} &= \bar{\mathbf{g}}^{n} + \mathbf{f}^{n} \\ &= \mathbf{R}_{e}^{n}(\mathbf{g}^{e} + \mathbf{\Omega}_{ie}^{e}\mathbf{\Omega}_{ie}^{e}\mathbf{r}^{e}) + \mathbf{f}^{n} \\ &= \mathbf{g}^{n} + \mathbf{R}_{e}^{n}\mathbf{\Omega}_{ie}^{e}\mathbf{\Omega}_{ie}^{e}\mathbf{r}^{e} + \mathbf{f}^{n} \end{aligned} \tag{1.6}$$

where $-\mathbf{\Omega}_{ie}^{e} \cdot \mathbf{\Omega}_{ie}^{e} \cdot \mathbf{r}^{e}$ is the centrifugal term of the Earth gravity field. Rearranging equation 1.6 yields the gravity vector expressed in the navigation frame:

$$\mathbf{g}^{n} = \mathbf{a}^{n} - \mathbf{R}_{e}^{n}\mathbf{\Omega}_{ie}^{e}\mathbf{\Omega}_{ie}^{e}\mathbf{r}^{e} - \mathbf{f}^{n} \tag{1.7}$$

or

$$\mathbf{g}^{n} = \mathbf{q}^{n} - \mathbf{f}^{n} \tag{1.8}$$

The acceleration vector $\mathbf{q}^{n}$ in equation 1.8 can be rewritten in terms of quantities obtainable from GPS measurements, namely the velocity vector given in the earth fixed frame and

projected to the navigation frame, $\mathbf{v}^n$, and it's time derivative $\dot{\mathbf{v}}^n$. The detailed derivation can be found in for example Britting (1971).

$$\mathbf{g}^n \approx \dot{\mathbf{v}}^n + (2 \cdot \boldsymbol{\Omega}_{ie}^n + \boldsymbol{\Omega}_{en}^n)\mathbf{v}^n - \mathbf{f}^n \tag{1.9}$$

Equation 1.9 is the basic equation for airborne gravimetry even it is an approximation. Substitution of (1.3) and (1.4) into (1.9) gives the equation in component form:

$$\begin{aligned} g_E &= \dot{v}_E - (\dot{\lambda} + 2\omega_{ie})\sin\varphi \cdot v_N + (\dot{\lambda} + 2\omega_{ie})\cos\varphi \cdot v_U - f_E \\ g_N &= \dot{v}_N + (\dot{\lambda} + 2\omega_{ie})\sin\varphi \cdot v_E + \dot{\varphi} \cdot v_U - f_N \\ g_U &= \dot{v}_U - (\dot{\lambda} + 2\omega_{ie})\cos\varphi \cdot v_E - \dot{\varphi} \cdot v_N - f_U \end{aligned} \tag{1.10}$$

The ellipsoidal coordinate rates are related to the e-frame velocity coordinatized in the n-frame, by:

$$\begin{aligned} \dot{\lambda} &= v_E / (N + h)\cos\varphi \\ \dot{\varphi} &= v_N / (M + h) \\ \dot{h} &= v_U \end{aligned} \tag{1.11}$$

where N and M are radii of curvature of the prime vertical and the meridian respectively. The values for N and M internationally adopted through the Geodetic Reference System 1980 (Moritz, 1992) will be used here. Substituting (1.11) into (1.10) gives the final component form of (1.9):

$$\begin{aligned} g_E &= \dot{v}_E + \left(\frac{v_E}{N + h} + 2\omega_{ie}\cos\varphi\right) \cdot (v_U + v_N \tan\varphi) - f_E \\ g_N &= \dot{v}_N + \left(\frac{v_E}{N + h} + 2\omega_{ie}\cos\varphi\right) \cdot \tan\varphi \cdot v_E + \frac{v_N v_U}{M + h} - f_N \\ g_U &= \dot{v}_U - \left(\frac{v_E}{N + h} + 2\omega_{ie}\cos\varphi\right) \cdot v_E - \frac{v_N^2}{M + h} - f_U \end{aligned} \tag{1.12}$$

The term $-(\frac{v_E}{N+h} + 2\omega_{ie}\cos\varphi)\cdot v_E - \frac{v_N^2}{M+h}$ is known as the Eötvös effect. Harlan (1971) gives a refined expression for this effect, which is more suitable for airborne gravity reduction than equation 1.12.

1.2 Strapdown vector and scalar gravimetry

The inertial sensors, i.e. gyroscopes and accelerometers, are in a strapdown system fixed to the body frame of the vehicle and maintenance of orientation is purely computational. This is in contrast to the mechanical gimbaled system, where the inertial sensors are isolated from the vehicle attitude changes.

Both factory-made Inertial Navigation Systems (INS) and dedicated custom-build systems are in use. The principles are the same; the accelerometers measure the specific forces in the body frame and the rotation matrix $\mathbf{R}_b^n$ converting from body frame to navigation frame is obtained from the gyroscopes. Equation 1.9 then reads:

$$\mathbf{g}^n = \dot{\mathbf{v}}^n + (2\cdot\Omega_{ie}^n + \Omega_{en}^n)\mathbf{v}^n - \mathbf{R}_b^n\mathbf{f}^b \tag{1.13}$$

The horizontal components of gravity are much more sensitive to misalignment and gyro errors than the vertical (Schwarz, 2001), and therefore less well determined. Kwon and Jekeli (2001) reports a noise level of 3 to 4 mgal for the vertical component and around 6 mgal for the horizontal components.

In the Strapdown Inertial Scalar Gravimetry (SISG) approach only the vertical component of equation 1.13 is interpreted as gravity. Glennie and Schwartz (1999) report accuracies at the 2 to 3 mgal level for their systems.

Bastos et al (2001) showed that also a low cost inertial measurement unit might be used to recover gravity. In this case the gyroscopes attitude control was aided by GPS observations from multiple antennas on the aircraft.

The length of the gravity vector may be accessed without any knowledge of the orientation of the sensors. Equation 1.8 can be rewritten as:

$$f^2 = (q^n - g^n)^2 \tag{1.14}$$

If the three accelerometers measuring the vector $\mathbf{f}$ are perpendicular to each other and the deflection of the vertical is ignored then equation 1.14 yields:

$$f^2 = f_1^2 + f_2^2 + f_3^2 = (q_U - g_U)^2 + (q_E - g_E)^2 + (q_N - g_N)^2 \approx (q_U + g)^2 + q_E^2 + q_N^2 \quad (1.15)$$

or

$$g = -g_U = \sqrt{f_1^2 + f_2^2 + f_3^2 - q_E^2 - q_N^2} - q_U \quad (1.16)$$

This is the principle for Rotation Invariant Scalar Gravimetry (RISG). The advantage of such an approach is that the gyros can be eliminated, which makes the system much simpler and cheaper. However, it appears that the SISG approach outperforms the RISG one. See Glennie (1999) for a detailed discussion of the RISG approach.

1.3 Stabilized platform systems

The most common mechanical stabilized system is the two-axis damped platform system. It is a mechanical gimbaled system, where a system of accelerometers, gyros and torque motors keep the vertical acceleration sensor more or less aligned with the plumb line. The most famous of the two-axis damped platform systems is the LaCoste & Romberg S meter. It has been widely used for marine and airborne applications. The vertical sensor is a heavily damped beam type gravimeter mounted on an inertial stabilized platform. Two torque motors keeps the platform horizontal. A feedback loop, with two horizontal accelerometers and two gyros gives the input signal to the torque motors, see Figure 1.1. The gyros control

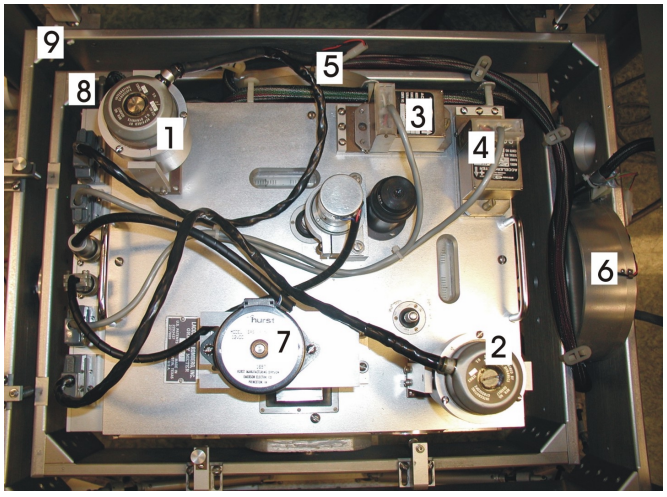

Figure 1.1. LaCoste & Romberg marine gravimeter. Top view.

1 & 2: long and cross axis gyros

3 & 4: long and cross axis accelerometer

5 & 6: long and cross axis torque motors

7: spring tension stepper motor

8 & 9: inner and outer gimbal frame

the short-term behaviour of the platform, while the horizontal accelerometers control the long-term level. In the absence of horizontal accelerations the platform is driven so that the accelerometer outputs are zero. That is the condition for the platform to be orthogonal to the gravity vector and gyro drift is automatically compensated. The principle and mechanization of the LaCoste & Romberg marine gravimeter platform is described in more detail in section 2.5.

The LaCoste & Romberg marine gravimeter has played a major role in the development of airborne gravimetry as an operational tool for gravity mapping. Tests were performed already in 1958 and showed that it was possible to determine mean gravity values for 100 km by 100 km blocks with an accuracy of 10 mgal (Thomson and LaCoste, 1960). The major problem was the accuracy of the navigation data in order to correct for the Eötvös effect and aircraft dynamics. During the next 3 decades several systems were tested. The aim was mainly to provide the oil industry with a tool for gravity mapping in areas difficult to access with traditional methods: see Gumert (1992) for an overview. Several additional aids for position determination were employed, but it was not until the advent of the GPS navigation system that the problem with accurate trajectory determination was really solved.

In addition to a higher accuracy, the GPS system also offered a worldwide coverage. The US Naval Research Lab pioneered airborne gravity mapping on a continental scale, taking advantage of the GPS system. A survey was flown over the entire Greenland in 1991 and 1992 (Brozena, 1992). The survey has since been extended to most of the Polar Ocean and has yielded new information on the tectonic structure and history of this area, see Childers et al. (2001).

Several companies and institutions perform airborne gravity surveys with stabilized platform systems today, both for geodetic, geophysical and exploration purposes. Fugro-LCT reports 0.7 mgal accuracy at 6 km half-wavelength resolution for their system based on a LaCoste & Romberg S-meter flown in a small fix-winged aircraft (Williams and MacQueen, 2001). Sander Geophysics reports similar results for their system, which is based on a three-axis gimbaled inertial navigation system and is also flown in a small fix-winged aircraft. The gravity sensor is a conventional inertial accelerometer (QA3000) operated in a temperature-controlled environment to minimize drift problems (Ferguson and Hammada, 2001). Both companies aim for customers in oil exploration.

National Survey and Cadastre – Denmark (KMS) has been active in airborne gravimetry since 1996. First in the frame of the AGMASCO project (Forsberg et al., 1996) and since

1998 in cooperation with The University of Bergen, Norway (UIB), see e.g. Olesen et al. (2002b). The main focus in the development of the KMS/UIB airborne gravity system has been to get a data quality adequate for geoid computation, i.e. data with the medium to long wavelengths virtually noise free, and at the same time get high-resolution data. The remainder of the present text is dedicated to the description, calibration and validation of the KMS/UIB airborne gravity system. The system is based on a LaCoste & Romberg marine gravimeter updated for airborne use.

1.4 Gravity equations relevant to stabilized platform systems

Since the stabilized platform under normal operational conditions will keep the gravity sensor axis close to an alignment with the gravity vector, it suffices to treat it as a one-dimensional case and estimate deviations from alignment as a first order approximation. The usual equation for gravity from a stabilized platform gravimeter (see e.g. Valiant, 1992) is in principle similar to the Rotation Invariant Scalar Gravimetry (RISG) approach as described in section 1.2 and will be referred to as the traditional approach in the following. Assume the stabilized platform system taking the role of the strapdown body system. With the two platform accelerometers in the near-horizontal plane, equation 1.16 reads:

$$\begin{aligned} g &= \sqrt{f_X^2 + f_Y^2 + f_Z^2 - q_E^2 - q_N^2} - q_U \\ &= \sqrt{f_X^2 + f_Y^2 + f_Z^2 - q_E^2 - q_N^2} - \ddot{h} + \delta g_{Eotvos} \\ &= f_Z - \ddot{h} + \delta g_{Eotvos} + \left(\sqrt{f_X^2 + f_Y^2 + f_Z^2 - q_E^2 - q_N^2} - f_Z\right) \\ &= f_Z - \ddot{h} + \delta g_{Eotvos} + \delta g_{tilt} \end{aligned} \tag{1.17}$$

The term δg_{Eotvos} is the Eötvös correction. An approximate expression can be derived from equation 1.12. Harlan (1968) gives, as mentioned earlier, an expression that is more appropriate for airborne applications.

δg_{tilt} is the correction for misalignment of the platform. As seen from the derivation of (1.17) the correction does not incorporate any explicit information about the platform tilt angles. As it will be shown in section 2.6 the platform tilt angles, i.e. the pitch angle χ and the roll angle η, can be modeled under the assumption that the deviation from level is small.

Equation 1.13 is then the starting point. The rotation in (1.13) is now from the sensor frame to the navigation frame. The sensor frame is defined so its axes are parallel to the navigation frames axes, when the aircraft is heading north and the platform is leveled. The attitude of the platform is given by the Euler angles α, χ and η, where α is the yaw angle of the aircraft. The rotation matrix then becomes (only the third row is of interest):

$$\mathbf{R}_{\mathbf{s}}^{\mathbf{n}} = \begin{bmatrix} r_{1,1} & r_{1,2} & r_{1,3} \\ r_{2,1} & r_{2,2} & r_{2,3} \\ -\sin\eta & -\cos\eta\sin\chi & \cos\eta\cos\chi \end{bmatrix} \tag{1.18}$$

The vertical component of (1.13) then reads:

$$\begin{aligned} g = -g_U &= -\ddot{h} + \delta g_{Eotvos} + \begin{pmatrix} -\sin\eta \\ -\cos\eta\sin\chi \\ \cos\eta\cos\chi \end{pmatrix}^T \cdot \begin{pmatrix} f_X \\ f_Y \\ f_Z \end{pmatrix} \\ &= f_Z - \ddot{h} + \delta g_{Eotvos} + (-\sin\eta \cdot f_X - \cos\eta\sin\chi \cdot f_Y - (1-\cos\eta\cos\chi)\cdot f_Z) \\ &= f_Z - \ddot{h} + \delta g_{Eotvos} + \delta g_{tilt} \end{aligned} \tag{1.19}$$

The estimation of the platform tilt angles χ and η is described in section 2.6. The key point in this approach is that the known platform properties are incorporated in the modeling of the tilt angles and thereby in the tilt correction; this is not the case in the traditional approach. This new way of estimating the tilt correction has proven to perform better than the traditional approach, for details see section 2.5 and 2.6.

The LaCoste & Romberg gravimeter is a relative instrument and the airborne measurements are tied to ground gravity values through stationary readings in the airport. This gives the actual gravity measurement at aircraft altitude as:

$$g = f_Z - \ddot{h} + \delta g_{Eotvos} + \delta g_{tilt} - f_{Z_0} + g_0 \tag{1.20}$$

where g_0 is the airport gravity value and f_{Z_0} is the corresponding still reading. The trajectory of an aircraft in level flight is characterized by regular variations in height and attitude known as phugoid motion. This is a basic consequence of aerodynamics and cannot be avoided. Equation 1.20 can be used to recover gravity, but because g depends strongly on

height and height variations are unavoidable, it may be advantageous to apply the final low-pass filtering to a quantity that is less height dependent than g. Both gravity disturbances and gravity anomalies are an option. Gravity disturbances may seem to be the most natural choice, since ellipsoidal heights are directly available from the GPS system. On the other hand, gravity anomalies are the most common derived product in other contexts. So for the sake of ease of comparisons and merging of the airborne data with other data sets, gravity anomalies are chosen to be the final product. The full reduction scheme for the airborne readings is then:

$$\Delta g = f_Z - \ddot{h} + \delta g_{Eotvos} + \delta g_{tilt} - f_{Z_0} + g_0 - (\gamma_0 + \frac{\partial \gamma}{\partial h} \cdot (h - N_{EGM96}) + \frac{\partial^2 \gamma}{\partial h^2} \cdot (h - N_{EGM96})^2) \tag{1.21}$$

As (1.21) shows, the reduction to gravity anomalies implies the incorporation of a geoid model in the processing scheme. EGM96 is used as the standard model (Lemoine et al., 1998). Gravity anomaly estimates as derived from equation (1.21) will contain a lot of rather high frequent measurement noise mainly induced by phugoid motion and by air turbulences. A low-pass filter is applied as the final step in the processing to reduce this noise to an acceptable level. It should be noticed that filtered gravity disturbances as well as filtered absolute gravity estimates can easily be derived from the filtered gravity anomalies.

2 The KMS/UIB airborne gravity system

System description and calibration are the main topics of this chapter. The gravity sensor response and the platform off leveling are treated in more details. Different error sources are identified and to some extent quantified.

The concept 'apparent K-factor' is introduced in order to access the combined response of the gravimeter and the GPS to vertical accelerations of the system and it is shown that the vertical sensor responds in a nonlinear way.

The bias behavior of the system is a key property, when it comes to geodetic use of the acquired data. Bias problems may be greatly reduced if known platform properties such as natural period are incorporated in the correction for off leveling effects. This is implemented by the new reduction scheme, which was formulated in section 1.4.

2.1 System setup

The gravity system has been installed in several aircraft since the first test flights in 1996; Dornier 228 (Skagerrak 1996), Casa Aviocar 212 (Azores 1997), Twin-Otter (Greenland/Svalbard 1998, 1999, 2000 and 2001 and Baltic Sea 1999) and Fokker F-27 (Great Barrier Reef 1999 and Corsica/Crete 2001). The key components have been the same; the LaCoste & Romberg S-99 gravimeter from UIB and two or more double frequency carrier phase GPS receivers. The gravimeter and the GPS receivers are installed as separate units; no sort of common data logging unit is in principle needed, since the phugoid motion provides a possibility for time synchronization by cross correlation, as outlined below. The gravimeter is installed under the wing near the symmetry plane to minimize

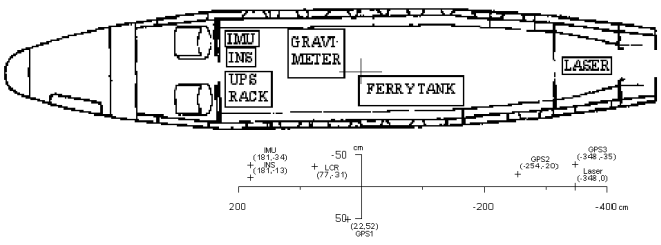

Figure 2.1. Left, sketch of the installation. Right, internal view of Twin-Otter installation looking forward in the cabin. Ferry tank to the left, LCR gravimeter to the right, and electronics rack in the background.

impact from aircraft maneuvers. For the installation of the GPS antennas the multi-path conditions and the horizontal offset from the gravimeter have been considered. The latter is of minor importance if the aircraft attitude variations are logged. Auxiliary equipment as a laser altimeter, an Inertial Navigation System or an Inertial Measurement Units has been installed in most cases. Figure 2.1 shows a typical installation in the Twin-Otter used for the Greenland, Svalbard and Baltic Sea operations. University of Bergen (UIB) owns the gravimeter while the rest of the equipment is KMS property.

2.2 Time synchronization. Validation by INS/GPS time tag

The gravimeter data are logged at 1 Hz and assigned an integer second time stamp, taken from the host computer clock. This sort of time tagging may serve well for shipborne gravimetry, but it is in general not good enough for airborne applications. The GPS data are also logged at 1 Hz, but have in contrast to the gravimeter data a very accurate time stamp. After some initial tests, with dedicated time tagging software aimed to improve the gravimeter time tagging, we realized that cross correlation techniques offer a simple and reliable way to synchronize the GPS and the gravimeter data. The GPS and the gravimeter data have a strong signal in common, the phugoid motion induced vertical acceleration of the aircraft. The correlation between the two signals is normally well above 90 %. The method is depicted in Figure 2.2 and works as follows. First the cross correlation function between GPS derived vertical acceleration and gravimeter reading is computed. The ordinate of the peak value is extracted from a graphical display of the correlation function and entered as a time shift to the gravimeter data. This is done iteratively until the correlation function peaks at exactly 0.0 seconds. The fractional part of the time shift is accomplished

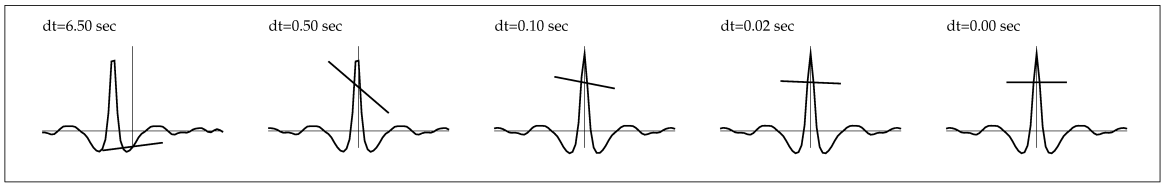

Figure 2.2. Cartoon, which illustrates the time synchronization procedure. First the integer number of seconds to shift the time series is determined from the offset of the peak value. The symmetry indicator, the more or less horizontal bar, then serves as a guide to determine the fraction of a second to shift the time series.

by linear interpolation of the gravimeter data. The symmetry indicator also shown in Figure 2.2 serves as a guide to determine the fraction of a second to shift the time series. This procedure may sound a bit tedious, but in the actual implementation it takes only a few seconds to estimate the optimal time shift for each track. The synchronization is done for each track, since the drift of the host computer clock is noticeable after a few hours.

The method works equally well on all data series with a strong signal in common. It has been applied both to the synchronization of gravimeter data, laser data and INS data with GPS data. The latter offers an opportunity to get an estimate of the accuracy of the method, since the INS data itself carries with it a very accurate time stamp derived from its integrated GPS unit. The vertical acceleration channel from the INS was synchronized with GPS derived acceleration as described for the gravimeter data and the assigned time compared with the time tag from its integrated GPS. This was done for the 14 separate tracks of the Corsica campaign flown in February 2001. The test is summarized in Table 2.1 and it shows that the synchronization is better than 50 milliseconds in all cases.

Table 2.1: Time synchronization test. Difference between INS/GPS time tag and cross correlation results (milliseconds).

No. of lines	mean value	Std. dev.	Minimum	Maximum
14	-20	20	-50	40

Table 2.2 shows that timing errors below 100 milliseconds has insignificant impact on the filtered gravity estimates. The results are from a profile with a high level of aircraft dynamics from the Greenland 2001 campaign. Such turbulent flight conditions are thought to be the situations most critical to time synchronization errors. The conclusion is that timing errors have only little impact on the quality of the filtered data from the airborne gravity system.

Table 2.2: The impact of synchronization errors on filtered gravity.

Synchronization error (millisec):	0	20	50	100	200	500
Mean of induced change (mgal):	0.00	0.01	0.03	0.09	0.32	1.77
RMS of induced change (mgal):	0.00	0.02	0.05	0.15	0.39	1.97

2.3 Vertical sensor calibration

The vertical acceleration sensor is based on the zero-length spring principle (Torge, 1989), also utilized in the LaCoste & Romberg land gravimeter. In the marine gravimeter the principle is implemented with an infinite sensitivity of the sensor, that is to say: the spring do not exert an extra restoring force on the beam, as the beam moves away from equilibrium. So when subject to any force not exactly balanced by the spring the beam will continue to drift.

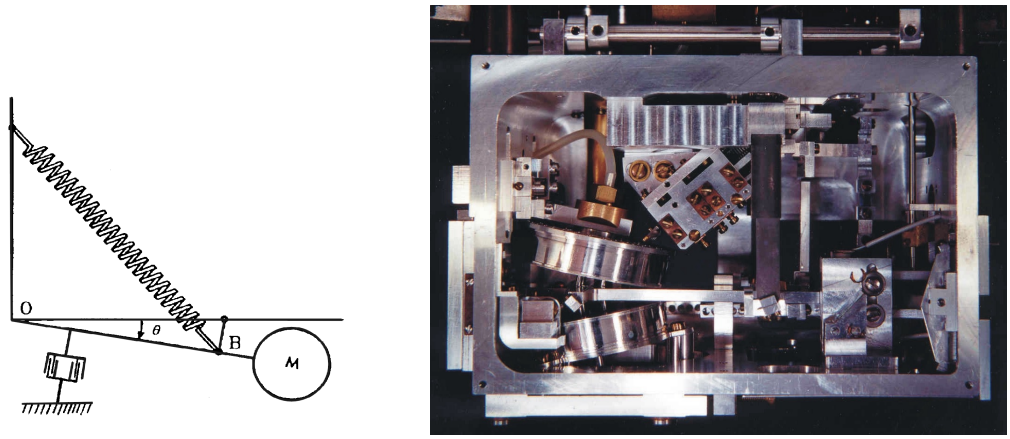

Figure 2.3. Left, sketch of the LaCoste & Romberg gravity sensor. Right, photo of the sensor interior.

Air dampers control the damping and hence the drift rate of the beam in the marine gravimeter, see Figure 2.3. The system is highly overdamped, which means that the response of the system is virtual instantaneous, for details see Valiant (1992). The equation for the motion of the beam is in its most general form the same as for other harmonic systems (LaCoste et al., 1967):

$$g + \ddot{h} + b \cdot \ddot{B} + f \cdot \dot{B} + k \cdot B - c \cdot S = 0 \qquad (2.1)$$

where g is gravity, $\ddot{h}$ the vertical acceleration exerted on the meter, B is the beam's deviation from equilibrium, $\dot{B}$ and $\ddot{B}$ time derivatives of B and $c \cdot S$ is the vertical force exerted by the spring. The factor k is zero for the LaCoste & Romberg marine meter (no restoring force) and f is due to the damping. If f is made very large and constant the beam will rapidly acquire its maximum velocity for a given unbalanced force acting on it and the term

$b\ddot{B}$ becomes insignificant. The approximate linear equation for the LaCoste & Romberg marine meter is thus (Valiant, 1992):

$$g + \ddot{h} + f \cdot \dot{B} - c \cdot S = 0 \tag{2.2}$$

The spring tension is slowly adjusted by a feedback loop to prevent the beam from drifting too far away from equilibrium. By measuring beam velocity $\dot{B}$ and spring tension S gravity readings can be done even when the beam is moving. The measurement becomes a combination of beam velocity and spring tension, and is to first order independent of beam position. The calibration factor c for the spring can be determined by making stationary readings at established gravity stations spanning a sufficient gravity range. The drift of the gravimeter, due to e.g. aging, must be accounted for in such a calibration.

Equation 2.2 is an approximation, and correction terms, known as **cross coupling**, are computed in real time. One of the correction terms relates directly to the non-linearity of the beam response and is proportional to the squared beam velocity (see section 2.4 for more details on cross coupling). The linearity of the S-99 meter was, after correcting for these terms, tested on several data sets. The tests all followed the same scheme. First the filtered gravity estimates along a test line were computed from the airborne measurements, then the unfiltered vertical acceleration derived from GPS together with Eotvos effect, tilt effect, spring tension and cross coupling terms was restored to give an estimate of the unbalanced specific force acting on the beam. This unbalanced force is plotted against beam velocity in Figure 2.4 for a single test line. The data points are seen to fall on an almost straight line, the slope of this line being the damping factor f from equation 2.2. There is a tradition of calling this factor for the **K-factor** and this tradition will be followed hereafter. The dispersion of the data points from a perfectly straight line can be explained by noise on both the GPS position estimates and the beam position readings. The time wise differentiation of beam position and GPS height component to get beam velocity and vertical acceleration will especially amplify the short period noise. If a low pass filter is applied to reduce this noise the data points fall on an almost perfect line (not shown). The puzzling observation is that the slope of the best fitting line, the K-factor, depends on the amount of filtering applied to the data. This is depicted in Figure 2.4. The longer the filter, the smaller the estimated K-factor. A linear response system where the K-factor is dependent only on the frequency and not on the amplitude of the driving signal, the unbalanced force, is one possible explanation,

but a nonlinear sensor response may as well be the explanation. Low pass filtering will tend to down-weight episodes with high amplitude accelerations, since such accelerations can persist only for a short period. So Figure 2.4 may equally well be interpreted as if the K-factor is dependent on the amplitude of the unbalanced force acting on the beam and hence dependent on the beam velocity, i.e. a nonlinear system.

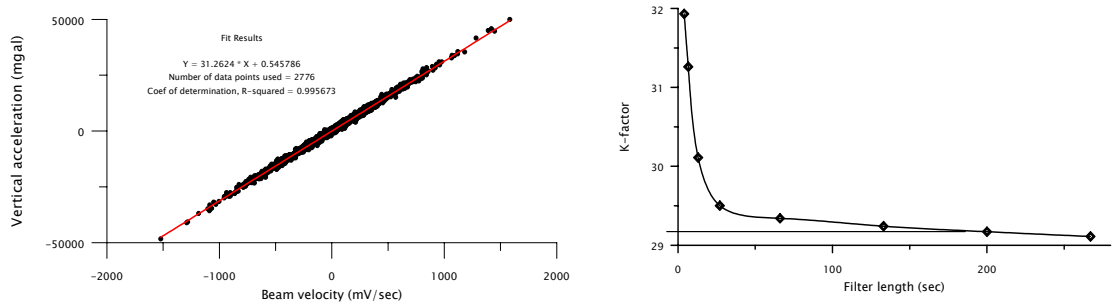

Figure 2.4. Left) estimation of apparent K-factor by linear regression. Right) the apparent K-factor's dependency on filtering.

To examine this observation in more detail, the K-factor's dependency on beam velocity and beam position was determined for a larger data set. The data are from the Greenland 2001 campaign. Some of the flights were quite turbulent adding high frequency power to the observations. The GPS signal was in general of a good quality. 64 hours of GPS and gravimeter data or 231,000 observations at 1 Hz were used in the analysis outlined below. A 5 second filter was applied to the data to reduce the impact of short period noise especially noise on the beam readings, before sorting the data into classes according to their beam velocity and beam position. An apparent K-factor was estimated by fitting a straight line, as in Figure 2.4, for each class. The velocity dependency for beam positions between –1000 mV and 1000 mV are listed in Table 2.3. Approximately 95 % of the observations fall within this band of beam positions.

Table 2.3: K-factor as function of beam velocity for beam positions between –1000 mV and 1000 mV. Beam velocities given in mV/sec

Velocity band:	→ -400	→ -200	→ -100	→ -50	→ -25	→ 0	→ 25	→ 50	→ 100	→ 200	→ 400 →
Mean velocity:	-465	-265	-139	-71	-36.1	-13.3	13.4	36.1	71	138	255	441
K-factor:	31.53	30.72	30.57	30.16	30.28	29.58	29.91	30.20	30.34	30.22	30.56	30.87

The table shows systematic changes in the K-factor estimates as the beam velocity changes. The K-factor increases with increasing beam speed. It should be noticed that the K-factor estimated this way, depends both on the gravimeter and the GPS derived accelerations, according to formulae 2.2. Any filtering, longer than 5 seconds, inherent from the GPS processing will impact the K-factor estimation. In the following the term 'apparent K-factor' will be used for this vertical-acceleration/beam-velocity relation.

Two approaches to model the beam response have been tested. The first one relates to Figure 2.4 and uses a constant K-factor that corresponds to the filter actually applied to the airborne data, which is between 180 seconds and 200 seconds. This will be referred to as the filter-optimized K-factor. The second model is shown in Figure 2.5 and is based on the observed apparent K-factors derived from the Greenland 2001 dataset mentioned previously. The beam velocity dependency is as in Table 2.2 and a parabolic term is added to account for the observed small variations with beam position.

Both approaches seem to perform equally well, when the normal filter length is used. The results discussed in chapter 3 can be achieved with both approaches. There is one difference however. The variable K-factor approach reduces the noise in the unfiltered gravity estimates to approximately 90% of the noise level for the filter-optimized K-factor approach. This indicates that such a modeling of the nonlinear response of the gravimeter beam may have the potential to improve the resolution of the airborne gravity system.

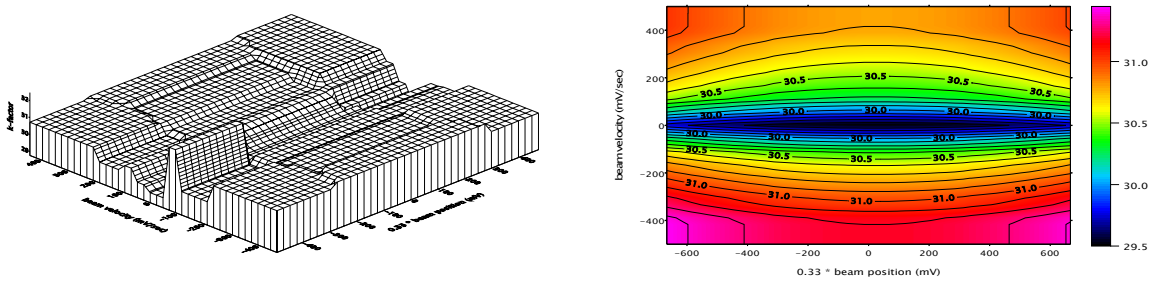

Figure 2.5. Apparent K-factor as a function of beam position and beam velocity. Left) observed K-factor. Right) model based on observations near equilibrium (95 % of the observations). A parabolic term is added to account for the observed small variation with beam position.

2.4 Cross-coupling. Linear least squares estimation over a pre-surveyed area

Traditionally the term cross coupling is used about a beam type gravimeter's sensitivity to horizontal accelerations (Torge, 1989). For the LaCoste & Romberg gravimeter more terms are lumped together in what is called the cross coupling correction. It is in addition to the traditional cross coupling, a real time modeling of the meters deviation from a linear response. Some of the terms are due to the lack of rigidity in the system and affects for example the centering of the air dampers under the presence of horizontal accelerations. The correction is computed as a linear combination of 5 so-called cross-coupling monitors (VCC, AX, AL, AX2 and VE, see Valiant, 1992). They are all products of beam position B, beam velocity $\dot{B}$ and horizontal accelerations f_x and f_y as measured by the gravimeter platforms cross and long accelerometers:

$$VCC \propto f_y \cdot B, \quad AX \propto f_x \cdot \dot{B}, \quad AL \propto f_y \cdot \dot{B}, \quad AX2 \propto f_x^{\,2} \cdot \dot{B} \quad \text{and} \quad VE \propto \dot{B}^2 \qquad (2.3)$$

The term VE relates to the discussion in the previous section. VE is proportional to the squared beam velocity and is used to model the non-linearity of the beam response. It may be sufficient in a marine application, but as shown in the previous section, considerable non-linearity is present in the beam response even after this correction has been applied.

ZLS Corporation, Austin, Texas, who did the upgrade of the gravimeter to airborne use, has determined the weight factors for the cross-coupling monitors from marine data series by a cross correlation technique. Such a determination will depend on the conditions under which the data are collected (LaCoste, 1973) and the determination may not be optimal for airborne use of the system. The airborne survey over the Skagerrak area performed in 1996, offers an opportunity to recalibrate the cross-coupling computation, since the gravity field in the area is well known from surface measurements, see Olesen et al. (1997). 15 hours of airborne data was used in a linear least squares adjustment of the weight factors. The weight factors were adjusted to minimize the difference between airborne data and upward continued surface data.

Table 2.4: Recalibration of cross coupling monitors. Comparison to surface data (mgal).

Monitors engaged:	none	VCC	AL	AX	AX2	VE	all
RMS difference:	2.68	2.64	2.62	2.58	2.68	2.61	2.56

Table 2.4 shows that only minor overall improvement is gained with this approach; the RMS error is reduced from 2.68 mgal with the old weight factors to 2.56 mgal when all weight factors are adjusted simultaneously. Even though the overall improvement is modest the recalibration can yield temporarily corrections of considerably magnitude as seen from Figure 2.6.

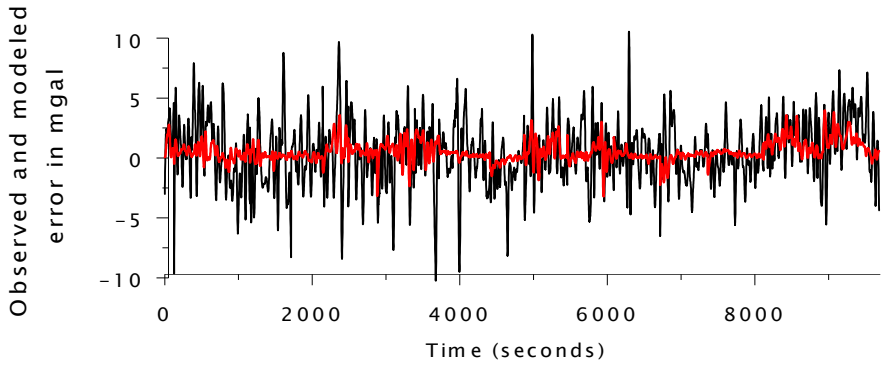

Figure 2.6. The effect of cross coupling modeling. The black curve shows the difference between airborne gravity and upward continued surface data from 15 hours of airborne measurements. Modeled additional cross coupling is shown as the red curve.

2.5 Frequency domain calibration of the horizontal accelerometers

The mechanization of the LaCoste & Romberg S-meter's stabilized platform is shown in Figure 2.7 for one axis. The platform is controlled by gyros via torque motors. A signal from the accelerometer is fed back to the gyros, to compensate for earth rotation and for changes in local level as the platform travels over the curved surface of the earth. The signal is a linear combination of the accelerometer output and its integral. This accelerometer feedback also compensates for gyro drift and initial platform errors, for details, see LaCoste (1967). This arrangement will keep the z-axis aligned with the gravity vector, in

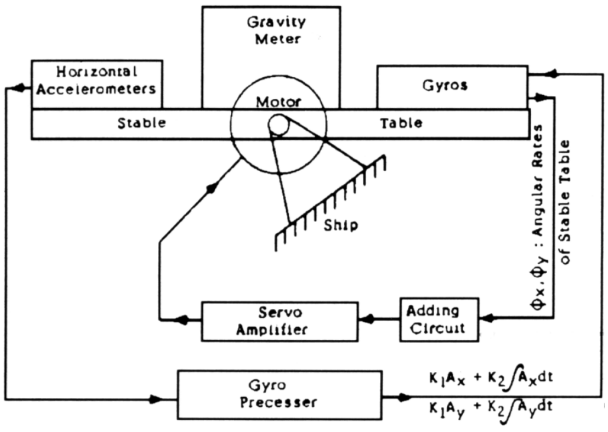

Figure 2.7. The platform feedback loop. Accelerometer output and it's integral combined with gyro output control the platform torque motors so equation 2.4 is satisfied.

the absence of horizontal accelerations.

Horizontal accelerations cannot be avoided in practice and severe errors may be induced from misalignment of the platform. The estimation of such errors is the subject of this section and of section 2.6.

The platform acts as a damped pendulum and the equation for the motion of the platform is, for one axis, given by LaCoste (1967) as:

$$\dot{\phi}_k + 2d\upsilon_0(\phi_k + \frac{a_k}{g}) + \upsilon_0^2 \int(\phi_k + \frac{a_k}{g})dt = 0 \tag{2.4}$$

where ϕ_k is the platform angular error and a_k is horizontal acceleration for one axis. υ_0 is the platform natural frequency, the term $2d\upsilon_0$ is the damping factor and g is gravity. The factor d is chosen so the damping is close to 0.707 times critical damping, which will minimize errors due to horizontal acceleration. The platform response to horizontal acceleration will depend on the frequency of the acceleration. The relation is given in the frequency domain as (LaCoste, 1967), (Swain, 1993):

$$\phi_k(\upsilon) = -\frac{\upsilon_0^2 + i2d\upsilon_0\upsilon}{\upsilon_0^2 - \upsilon^2 + i2d\upsilon_0\upsilon}\frac{a_k(\upsilon)}{g} \tag{2.5}$$

The horizontal accelerometer will for small angles ϕ_k sense almost the full impact of horizontal acceleration and a fraction of gravity. The accelerometer output can thus be written in the spectral domain as (Olesen et al., 1997):

$$\begin{aligned} f_k(\upsilon) &= g \cdot \sin(\phi_k(\upsilon)) + q_k(\upsilon) \cdot \cos(\phi_k(\upsilon)) \\ &\approx g \cdot \phi_k(\upsilon) + q_k(\upsilon) \\ &= -\frac{\upsilon^2}{\upsilon_0^2 - \upsilon^2 + i2f\upsilon_0\upsilon} \cdot q_k(\upsilon) \end{aligned} \tag{2.6}$$

where f_k is accelerometer output for the k'th axis. Figure 2.8 shows the amplitude of this theoretical platform behavior together with the observed relation. It is seen from Figure 2.8, that the platform acts as a high-pass filter towards horizontal accelerations. This way of displaying the horizontal acceleration components gives good insight into the platforms behavior, e.g. actual platform period and the healthiness of the platform control system. It is also a good way to determine calibration factors for the horizontal accelerometers on in-

flight data, due to the constant value of the transfer function at higher frequencies. Another way to state the platform spectral behavior is to say that it fully compensates for long period horizontal accelerations whereas it is insensitive towards short period impacts. It is seen from Figure 2.8 that the off-level or tilt angles have no spectral components above approximately 0.01 Hz. This is an important observation and it is utilized in the next section to derive a correction term for the off-leveling errors that is linear in the horizontal accelerations.

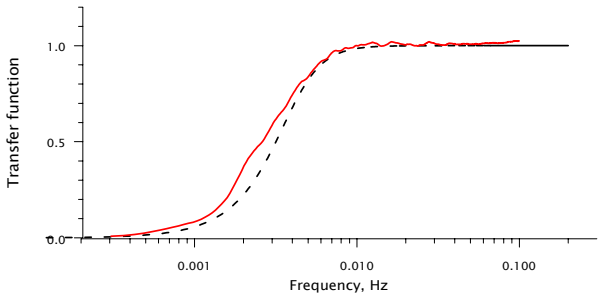

Figure 2.8. Theoretical (black/dashed) and observed (red/solid) platform accelerometer response for one axis.

2.6 Tilt effect and biases. A new platform modeling approach

The effect of a tilting platform is both to make the gravimeter less sensitive in the vertical direction, and to make it sensitive to horizontal accelerations. The traditional approach (the RISG-like approach) to account for this effect leads to a correction term that is non-linear in the accelerations. The correction term is derived in section 1.4 as:

$$\delta g_{tilt} = \sqrt{f_x^2 + f_y^2 + f_z^2 - q_E^2 - q_N^2} - f_z \qquad (2.7)$$

where f_k denotes accelerations measured by the gravimeters three accelerometers and q_k denotes horizontal kinematic accelerations derived from GPS and defined by (1.8) and (1.12). Valiant (1992) gives an approximate expression derived from (2.7) under the assumption that $f_z \cong g$ and $g >> f_{x,y}$:

$$\delta g_{tilt} = \frac{f^2 - q^2}{2g} \tag{2.8}$$

where $f^2 = f_x^2 + f_y^2$ and $q^2 = q_E^2 + q_N^2$. The last equation is good in the sense that it highlights the problem with the tilt correction. It is basically a small difference between two potentially huge numbers. Furthermore, the two potentially huge numbers are derived by squaring discrete and very noisy measurements. In addition to that, the noise on the separate terms must be expected to have different signatures, so the noise on the squared terms is not likely to cancel out due to the subtraction. Such an approach will certainly cause problems, problems that cannot be filtered out by the final low pass filter, since the squaring will change the characteristics of the noise signal. A zero-mean noise will after the squaring have a positive mean value. In this way the tilt correction may become a way for zero-mean noise to bias the gravity estimates. Pre-filtering of the data before the tilt correction is derived may reduce the problem, but the optimal amount of filtering is somewhat ambiguous.

The tilt angles may alternatively be estimated from the combined gravimeter and GPS observations. For small tilt angles the following approximations hold for one axis, see also Figure 2.9:

$$f_x = q_x + \sin(\phi) \cdot f_z \approx q_x + \phi \cdot f_z \approx q_x + \phi \cdot g \tag{2.9}$$

or

$$\phi \approx \frac{f_x - q_x}{g} \tag{2.10}$$

It was shown in the previous section that the tilt angle has no spectral components above approximately 0.01 Hz. With this knowledge the tilt angles can be well modeled and filtered. High frequency noise in the tilt angle estimation can be effectively removed with a low-pass filter that matches the platform period. This leads to the computation of the tilt correction being split into two parts, (i) the modeling of a physical system with known properties (the stabilized platform) and (ii) the correction for tilt

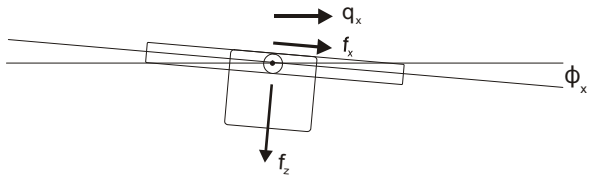

Figure 2.9. Tilting platform.

computed as a linear combination of three acceleration components:

$$\delta g_{tilt} = (1 - \cos(\phi_x) \cdot \cos(\phi_y)) \cdot f_z + \sin(\phi_x) \cdot f_x + \sin(\phi_y) \cdot \cos(\phi_x) \cdot f_y \qquad (2.11)$$

This implies, that zero-mean noise on the acceleration estimates will propagate unbiased as zero-mean noise into the tilt correction and will therefore not induce any bias into the gravity estimates.

Table 2.5 shows the performance of the two different tilt correction algorithms. Two tracks from the Greenland 2001 survey are analyzed, where one track was flown under turbulent conditions and the other was flown under smooth conditions. It is seen that the two algorithms yield the same results when no filtering is applied. This should not surprise, since the two methods are identical in that case. The table shows a dramatic change in mean value when filters are applied, especially for the dynamic flight, from 13.3 mgal to –2.1 mgal for the traditional approach, when a 1 seconds filter is applied before calculating the correction. Further filtering is seen to change the mean value several mgal, when we still look at the traditional approach. This shows that the tilt correction can add severe biases to our data, as it is unclear which amount of filtering is optimal. Moreover, the optimal filter length may change due to the dynamics of the flights. The modeling approach, on the other hand, is seen to be much less filter-sensitive for realistic filter lengths. Besides, the optimal filter length is more or less given from the previous section. A filter around 60 to 80 seconds should be adequate.

Table 2.5: Comparison of the two different tilt correction algorithms.

Traditional approach					Modeling approach				
Pre-filter	Quiet flight		Dynamic flight		Platform filter	Quiet flight		Dynamic flight	
	Mean	St dv	Mean	St dv		Mean	St dv	Mean	St dv
0 sec	0.32	1.49	13.26	8.42	0 sec	0.34	1.48	13.30	8.42
1 sec	-0.46	0.97	-2.09	4.29	20 sec	-1.01	0.93	-5.46	4.06
2 sec	-0.76	0.91	-3.87	3.92	40 sec	-1.02	0.93	-4.48	4.01
3 sec	-0.88	0.89	-3.98	3.75	60 sec	-0.99	0.95	-4.26	4.18
5 sec	-0.92	0.86	-3.64	3.47	80 sec	-0.98	0.95	-4.18	4.37
10 sec	-0.87	0.77	-2.82	2.81	100 sec	-0.98	0.95	-4.03	4.32
20 sec	-0.77	0.61	-1.84	1.83	120 sec	-0.97	0.95	-3.79	4.20

The standard deviation of the tilt correction in Table 2.5 shows somewhat the same dependency on filter length as does the mean value. But, the mean value is the main concern for us, as the data are intended for geodetic use. The modeling algorithm described in this section is a more sound way to establish the correction for platform errors, than is the traditional algorithm. The modeling approach incorporates the known physical properties of the platform system in its algorithm in contrast to the traditional approach.

2.7 GPS related errors. Cycle slip detection

Good acceleration estimates from GPS are essential for airborne gravity. Relative position accuracies at the centimeter level are required to obtain acceleration accuracies at the mgal level after filtering, see e.g. Czombo (1994) for a discussion of the spectral signature of GPS errors and the related impact on the filtered gravity estimates. The required absolute position accuracy is more relaxed and it is determined by the free air gradient (0.3086 mgal/m) and 0.5 m will be satisfactory for most applications. Normally this is obtained routinely with careful use of commercial GPS processing software for baselines up to several hundred kilometers (Forsberg et al., 1999).

The main problems arise from cycle slips, when the receiver looses lock on the signal due to (for example) ionospheric scintillation or to the inclusion of new satellites in the observations. This may induce position jumps with the magnitude of one or a few wavelengths, in fixed ambiguity type solutions. It is essential to identify such jumps, since after filtering they are easily interpreted as gravity anomalies. It is not possible to identify the jumps directly from the position estimates, due to the dynamics of the flight, but analysis of the unfiltered gravity estimates can help to identify them.

Figure 2.10 gives an example of how raw gravity estimates can be utilized for cycle slip detection and repair. The raw gravity signal has an RMS-amplitude of a few thousand mgal; such a value indicates smooth flight conditions. The raw signal often reaches an RMS value of 10000 to 15000 mgal under more turbulent conditions. There is a distinct exception around 6800 second, where the signal has a peak value of 40.000 mgal and one second later the value is minus 40000 mgal. A sudden jump in the GPS height component of 40 cm could explain the signal. 40 cm corresponds to approximately two wavelengths for the GPS carrier wave. The GPS trajectory is a so-called fixed ambiguity solution type, which causes the error related to the ambiguity fixing to be of a discrete nature, i.e. to be a multiple of the

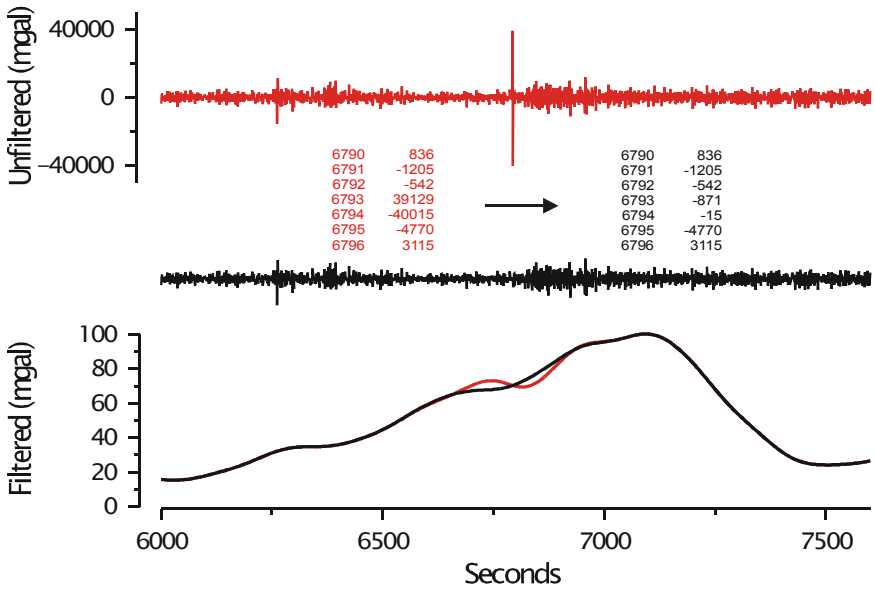

Figure 2.10. Cycle slip detection and repair. Upper graph is unfiltered gravity anomaly. Lower graph is filtered anomaly. Red is before and black after repair of presumed cycle slip. A plus/minus 40000 mgal signal has been removed from the unfiltered series.

L1 wavelength. The repair of this presumed cycle slip induced acceleration peak is seen to yield a more smooth filtered gravity signal. A dipole signal with amplitude of 2.5 mgal has been removed. The high frequency (1 Hz) nature of the error signal coming from jumps in the position estimates is the reason for the filtered error to have a relative small magnitude. Even though the error signal is small it may have significance in the case where the data are used for geophysical interpretation. If more than one position jump occurs within a filter length, the combined effect on filtered gravity can be considerably larger than the example shown in Figure 2.10.

If other vertical acceleration estimates are available, they may be used as well. Both the vertical accelerometer output from a strap-down inertial measurement unit (IMU) and laser altimetry over open water has proven to be a valuable help in the search for cycle slip induced position jumps.

Comparisons between GPS derived vertical accelerations and accelerations derived from laser altimetry on days with little wind and thereby a calm sea may give an indication of how much GPS contribute to the noise budget. The filtered difference of the two acceleration estimates was in general around 0.4 to 0.5 mgal RMS under such conditions, i.e. less windy days of the 1999 Baltic Sea and the 1996 Skagerrak survey. This comparison gives an upper limit on the noise on the vertical acceleration estimates. If the GPS noise is uncorrelated

with the other error sources, mainly gravity sensor noise, the contribution from GPS to a total noise budget of 1.5 mgal is only 3 to 4 percent. These results are obtained with relatively short baselines for differential GPS (less than 400 km) and with settled ionospheric conditions, so the relative importance of GPS noise on the data obtained in the arctic region during the years of 1998 to 2001 could be considerably larger.

2.8 Lever arm effect

A horizontal offset between GPS antenna and gravimeter will cause a so-called lever arm effect, i.e. the vertical acceleration experienced by the GPS antenna will be different from that experienced by the gravimeter due to aircraft attitude variations. This will induce a small noise signal in the derived gravity estimates. The effect can be sufficiently modeled if aircraft attitude information is available from an inertial navigation system or measurement unit or can be neglected if the offset between GPS antenna and gravimeter is small.
The instrument offset were rather large, 7.2 m, for the 2001 Corsica campaign due to installation constraints. The RMS value of the filtered lever arm effect was 0.4 mgal for all Corsica flights, with an absolute maximum of 1.6 mgal as modeled from attitude data. So for offsets less than 1 meter, the effect can safely be neglected.

2.9 Filtering and achievable resolution

The main purpose of filtering is to reduce the extreme high noise level on airborne gravity readings. The vertical acceleration of the aircraft often reaches 50000 mgal (RMS). This is a mean value for a whole track; peak values of several hundred thousands mgal are not uncommon. Most people find such flight conditions quite unpleasant. Measurements under such conditions will give noisy data no matter how well all known effects are modeled. The challenge is to leave as little noise as possible in the unfiltered gravity estimates and hence get away with a shorter final low pass filter. Common RMS values for unfiltered gravity anomalies are typically 2000 mgal to 5000 mgal for low-turbulence conditions and up to 20000 mgal for more turbulent conditions; such noise levels will fully mask any real gravity anomaly. It is mainly high frequency noise and low-pass filters can effectively reduce the noise level. The amount of filtering to apply is a trade off between spatial resolution and accuracy. A short filter yields a good spatial resolution at the expense of measurement noise

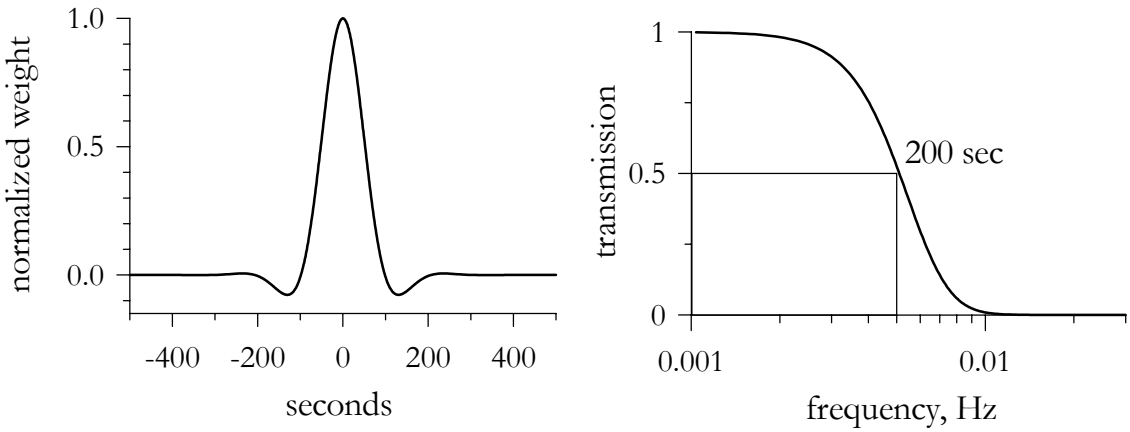

Fig. 2.11. Normalized convolution filter (left) and transfer function (right) for a typically used gravity filter. Half transmission point at 200 seconds.

and vice versa. The filter shown in Figure 2.11 is the standard filter applied to the airborne data at KMS. It is a six-fold cascaded second order Butterworth filter implemented as a sequential routine in the time domain, see e.g. Kanasewich (1975). It is applied forwards and backwards in time to avoid the introduction of time lags, i.e. a zero-phase filter. The filter could equally well have been implemented in the frequency domain. The half transmission point is around 0.005 Hz as seen from the spectral representation in Figure 2.11. This corresponds to a 100 seconds half-wavelength/half-amplitude resolution, or approximately 6 km with a ground speed of 60 m/s (120 knots). It should be noted that the filter has a relative steep roll-off compared to filtering based on e.g. cascaded RC-filters, i.e. anomalies characterized by half-wavelengths just above 6 km are recovered with almost full amplitude by the present filter. This filter property should also be considered when comparing the resolution of various airborne gravity systems.

Both GPS and gravimeter contribute to the noise budget. Results from flights over a smooth sea surface indicate, as mentioned in the previous section, that the gravimeter dominates the noise picture. The Skagerrak campaign was partly flown over a rather well surveyed sea and offers thus an opportunity to study this observation in more details. The laser altimeter operated along with the gravity system gives an independent estimate of the height variations and thereby the vertical accelerations of the aircraft. The fact that the altimeter readings yield aircraft altitude referred to sea level rather than to the ellipsoid has insignificant impact on the acceleration estimates. Table 2.6 and Figure 2.12 show results from a flight with very calm sea conditions. The difference between GPS and altimeter

derived vertical acceleration gives an upper band on how much GPS contribute to the noise under the actual conditions. The gap of approximately 1.5 mgal between gravity error estimate and GPS noise can only in part be ascribed to errors in the upward continued gravity field used to estimate the gravity error. A substantial part of this difference must be ascribed to the gravimeter modeling. So there seems still to be some potential for improvements, either in terms of a better modeling of the sensor response or in terms of a better vertical sensor. This is at least the conclusion under such relative favorable conditions, i.e. short base lines for DGPS (less than 300 km in this case), settled ionospheric conditions and little turbulence. Figure 2.12 also shows that the 200 seconds filter can be shortened considerably with only minor increase in the noise level as a consequence. A filter length of 110 seconds corresponding to a half-wavelength/half-amplitude resolution of 3.3 km will yield data with a noise level below 2.6 mgal. Again this is the case when considering smooth conditions; to achieve a good accuracy for a wide range of flight and ionospheric conditions a longer filter is needed.

Table 2.6: GPS noise

Filter length (sec)	GPS/laser difference (mgal)	Gravity error (mgal)
50	7.2	8.9
60	4.3	6.6
80	2.1	3.5
100	1.2	2.8
120	0.8	2.4
150	0.5	2.0
200	0.4	1.8
300	0.3	1.5

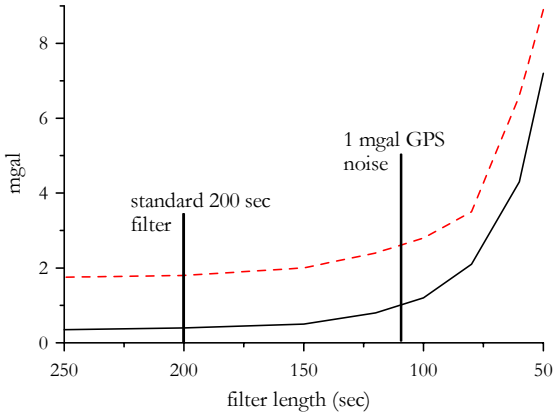

Figure 2.12. Difference (RMS) between airborne and upward continued surface data (red/dashed) and between GPS vertical and laser altimeter derived acceleration (black/solid). The latter gives an upper band on how much GPS contribute to the total noise budget for the airborne gravity data. 110 seconds filter length is seen to correspond to 1 mgal GPS/laser noise.

3 Survey descriptions and discussion of results

The background for the different surveys is briefly presented and the data accuracy is accessed. The survey data has not been subject to any sort of crossover adjustment to minimize the misfit at line crossings and the results from crossover analysis are therefore a realistic estimate of the data accuracy. Accuracy estimates obtained this way appears to be consistent with comparisons to surface data.

Data accuracies range from 1.3 to 2.0 mgal at 6 km resolution for the separate years of the Greenland surveys. The Baltic survey yielded data accurate to 1.4 mgal. These surveys were all flown with a Twin-Otter. The Great Barrier Reef, the Crete and the Corsica surveys were flown with a Fokker F-27, a bigger aircraft, and yielded accuracies from 2.5 to 3.0 mgal.

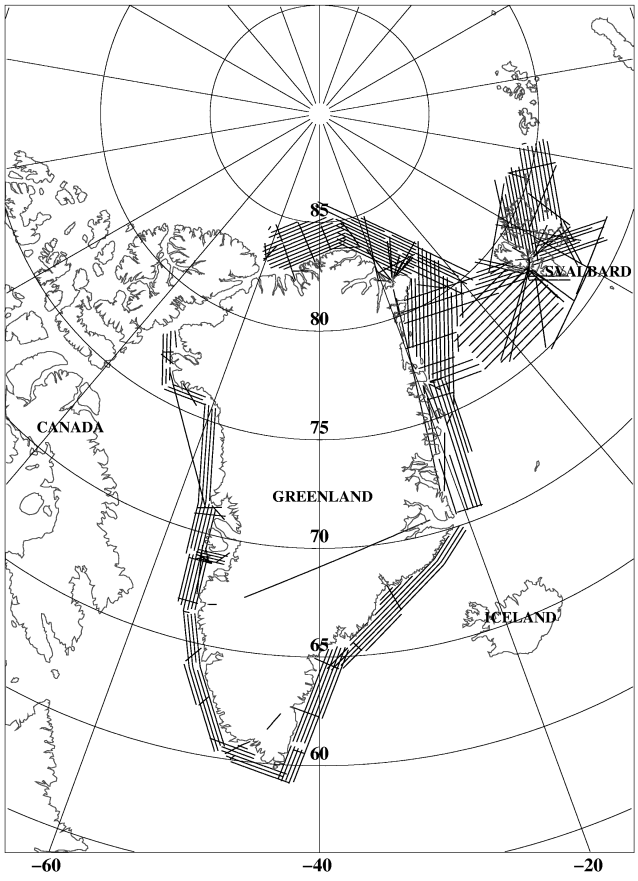

Fig. 3.1. Ground tracks for the Greenland surveys. Additional tracks around Svalbard flown in cooperation with Statens Kartverk, Univ. of Bergen and a Norwegian oil company are also shown.

3.1 The Greenland surveys

The airborne gravity surveys around Greenland were performed during four field campaigns during the summers of 1998 to 2001 (Forsberg et al., 1999, Olesen et al., 2002b). The purpose of the surveys was to complement the existing on-shore gravity coverage, mainly established by KMS by helicopter-based conventional gravimetry in the years of 1991-1997 (Forsberg and Rubek, 1998).

All offshore flights have been low level, i.e. between 100 and 250 m above sea level, so the effect of upward continuation is rather insignificant and airborne and surface gravity anomalies may be compared directly.

Table 3.1 summarizes the crossover error statistics for the four years of measurements. A total of 489 line crossings yielded a 2.5 mgal RMS difference. This number indicates a 1.8 mgal noise level on the separate tracks (2.5 mgal divided by square root of 2), under the assumption that the noise is uncorrelated between tracks. The error distribution plotted in Figure 3.2 follows pretty well a normal distribution with a standard deviation of 2.5 mgal and supports thereby the assumption of an uncorrelated noise signal.

Table 3.1: Crossover statistics

Data set	No of crossings	RMS (mgal)	Max (mgal)
1998	86	1.8	4.5
1999	74	2.5	8.6
2000	96	2.8	9.3
2001	66	2.6	8.2
All years	489	2.5	9.3

It is common practice to subject marine and airborne profile data to an adjustment procedure that minimizes the misfit at the crossing points, either as a linear trend or a bias removal. It may be justified to do this to marine data, see LaFehr and Nettleton (1967) for a discussion, but for airborne data obtained with a long-term stable gravimeter like the LaCoste & Romberg meter and a proper reduction for motion induced effects there seems to be little physical justification for such an adjustment. The gravimeter is virtual drift-free during the short time span of a flight, so bias or tilt problems in the data may indicate that the processing algorithm is less than optimal. The situation is different for systems utilizing sensors, which are known to drift, such as INS equipment, but it doesn't make the crossover adjustment healthier. Any crossover adjustment will by nature distribute point errors at crossing points into along-track corrections, and thus provide a way for short-period random errors to leak into longer wavelengths. For these

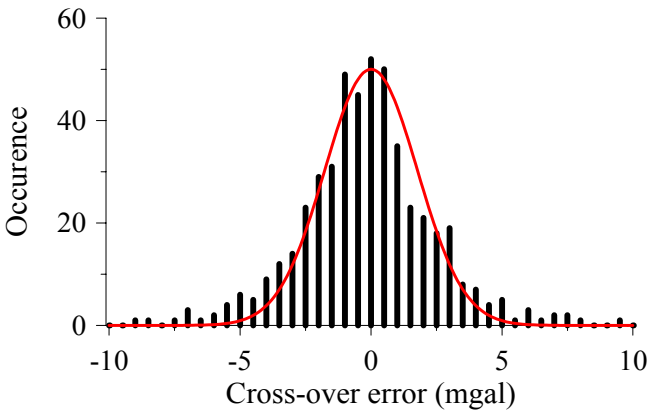

Figure 3.2. Crossover error distribution (vertical bars) and a normal distribution with a 2.5 mgal standard error (in red)

reasons it was decided not to apply crossover adjustment to the airborne data, but instead address the processing of the data, in order to identify where biases may be introduced. Section 2.5 and 2.6 gave a review of these efforts see also Olesen et al. (2002a).

The year 1998 gave considerably better results as judged from the crossover errors than the other three years; 1.8 mgal RMS crossing error indicating a noise level around 1.3 mgal. Good weather conditions are likely to be the reason; the 1998 flights were considerably less turbulent than the other years. More settled ionospheric conditions in 1998 might also have played a role.

Table 3.2 shows a comparison of the airborne data to nearby proprietary marine data distributed along large sections of the coast. The marine gravity data were collected from 1991 to 1997 by NUNAOIL, the national oil company of Greenland, on behalf of a group of international oil companies. The data is considered to be of a very high quality, with an error standard deviation of less than 1 mgal. A special effort was made to ensure that the marine data were properly connected to IGSN71 (Strykowski and Forsberg, 1995). The noise estimates obtained from the crossover analysis seems to be consistent with the comparison to marine data. The latter indicates a noise level for the airborne data around 2 mgal, as based on the 2.5 mgal and 2.7 mgal standard deviation difference to interpolated marine points within 1 km and 2 km respectively. Not only the airborne data but also the lateral gravity gradients and noise in the marine data contribute to this difference. Comparisons to sea ice gravity data gathered by Canadian agencies in the Polar Sea indicate a somewhat lower noise level for the airborne data. This observation fits well with the fact that those airborne data are from the 1998 survey, which had a smaller crossover error.

Table 3.2. Comparison to surface data within 2 km from the airborne tracks

Unit: mgal	Max. dist.	No of points	Max. diff.	Mean diff.	Std. dev.
NUNAOIL	2 km	2455	14.7	0.5	2.7
marine data	1 km	1212	13.1	0.4	2.5
Canadian ice data	2 km	27	2.6	0.6	1.4
Polar Sea	1 km	12	2.2	0.4	1.3

The mean differences of 0.4 mgal for marine data points within 1 km from the airborne tracks indicate that one or both of the data sets contain minor systematic errors. The harbor gravity ties are a possible partial source for such an error for the marine data sets, e.g. due to

un-modeled terrain effects of the quay or insufficient tidal modeling. Also, the EGM96 geoid model incorporated in the airborne data sets may be a source for minor systematic errors; this may in particular be true for the northern most areas where very little data were available for the determination of the EGM96 geoid model, see Lemoine et al. (1998).

3.2 The Baltic Sea

This survey was undertaken in September 1999 in cooperation with the Geodetic Surveys of Sweden and Finland, the Geological Survey of Sweden and the Geodetic agencies of Estonia, Latvia and Lithuania. The Baltic Sea represented until then a major gravity void with only little and scattered data available and it was decided to try to fill in airborne data in order to improve the situation for geoid computations. The crossover error statistics for the Baltic survey indicates a noise level around 1.4 mgal, almost the same as the 1998 Greenland survey. Flight conditions were smooth to moderate turbulent over the sea and quite turbulent over land. As for the Greenland surveys the noise estimates from crossover

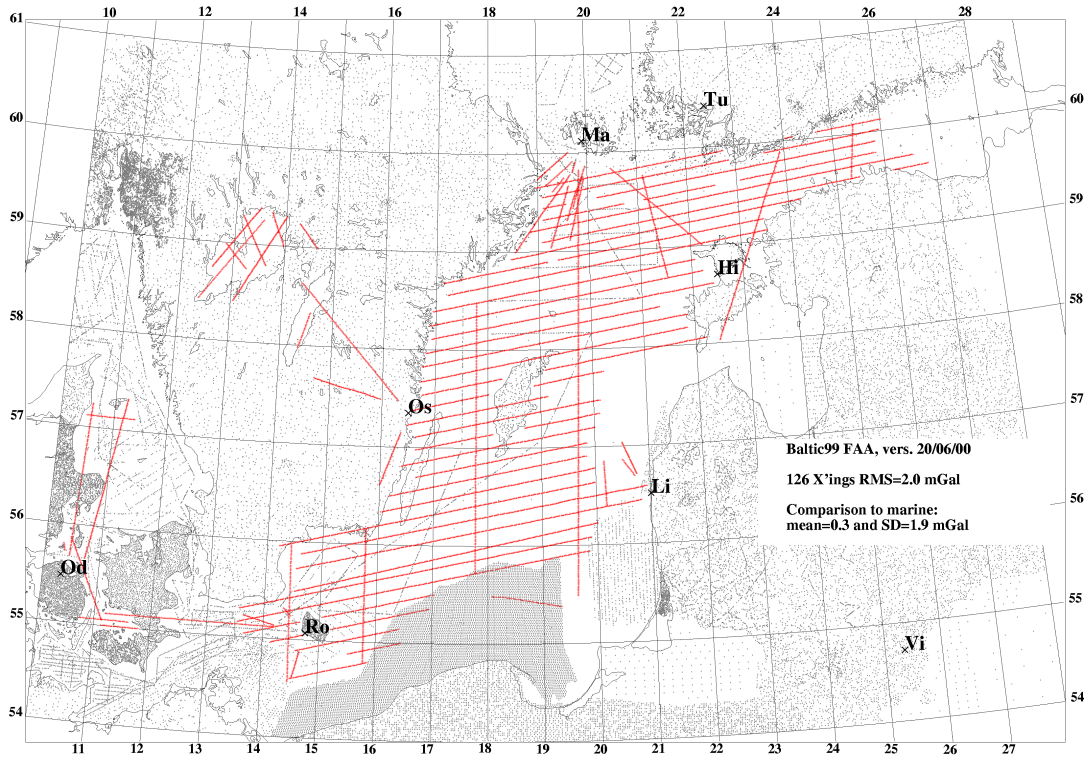

Figure 3.3. The Baltic Sea airborne gravity survey. Airborne data shown as red dots, available surface data as gray dots. Also shown the location of the GPS reference stations.

analysis and from comparisons to surface/subsurface data seems to be consistent, see Table 3.3 and 3.4.

Table 3.3. Baltic Sea crossover statistics

No of crossings	Max. difference	RMS difference
126	8.4 mgal	2.0 mgal

Table 3.4. Comparison to marine/submarine data sets

Data set	No of points	Mean difference	Std. dev. of diff.
Haakon Mosby	>500	-0.5	1.9
Polish marine	>100	0.0	1.2
Latvian submarine	>50	1.1	1.9

3.2 Great Barrier Reef, Corsica and Crete campaigns

The Great Barrier Reef, the Corsica and the Crete surveys where all flown with a Fokker F-27, a somewhat bigger aircraft than the Twin-Otter. After the first flights of the Great Barrier Reef campaign in October 1999 it became clear that it also had a quite different phugoid motion spectrum with much more long period power than the Twin-Otter. The longer periods of this phugoid motion fell within the pass-band of the desired filter and induced a noise signal in the filtered gravity estimates. This called for a more thorough investigation of the gravimeter beam response and led to the modeling described in section 2.3.

Besides yielding new valuable data in what was up to then a major gravity void, the Great Barrier Reef Airborne Gravity campaign also demonstrated the feasibility of performing airborne gravity measurements along with other measurements as bathymetric charting, see Olesen et al. (2001).

Deficiencies in the existing gravity coverage around Crete and Corsica have tampered geoid computations in these areas for a long time (Arabelos et al., 1994). The marine data is somewhat scattered and in part of a doubtful quality. In the near coastal regions, the accuracy of gravity models derived from satellite altimetry is known to degrade, due to the coastal sea state variability (Andersen and Knudsen, 2000). The altimetric gravity model used for comparison here is the KMS99 model (Andersen et al., 2001). The processing of the satellite altimetry data is based on the EGM96 geoid, and possible deficiencies in the

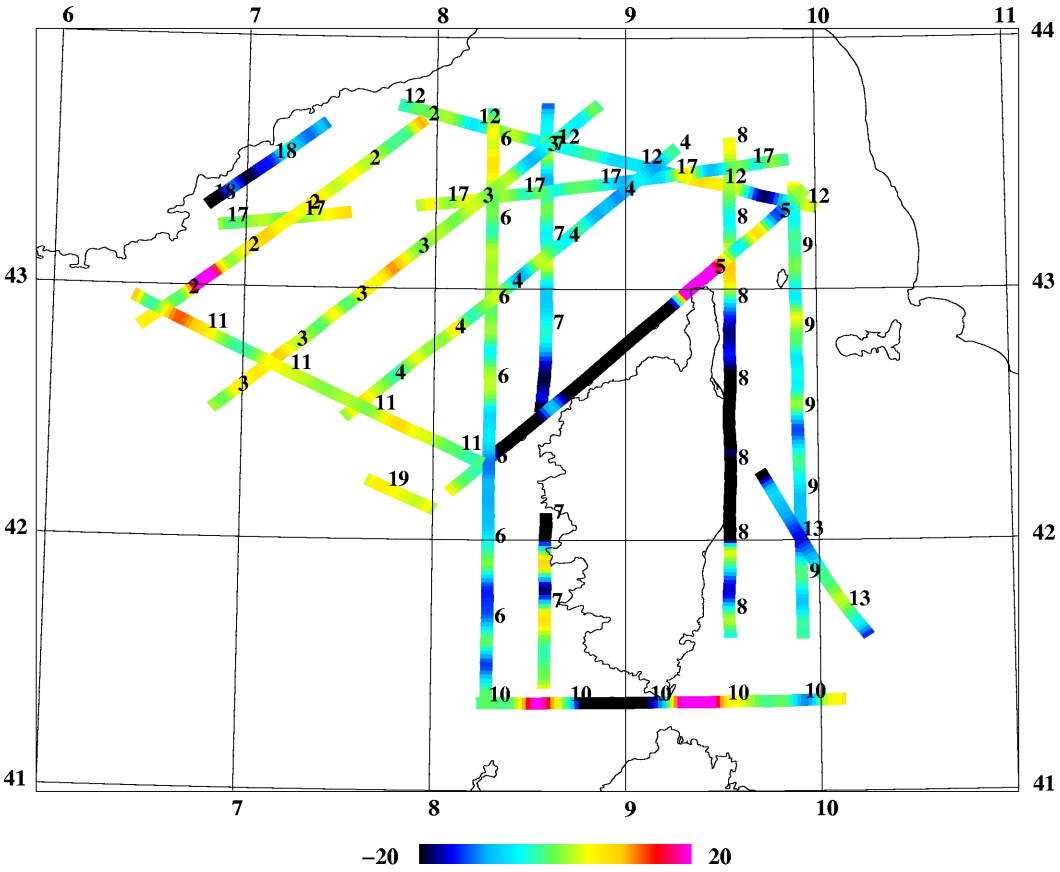

Figure 3.4. Difference between airborne gravity and the KMS99 gravity model derived from satellite altimetry. The airborne lines are labeled with ID number.

EGM96 geoid of wavelength longer than 200 km will not be improved from the altimetric observations. This may lead to long wavelength errors in the altimetry derived gravity field in addition to the near-coastal problems. The difference between airborne gravity and satellite altimetry based gravity depicted in Figure 3.4 underlines the need to be critical towards altimetric gravity fields in near-coastal regions. Severe discrepancies, up to 50 mgal, are observed along most of the coast of Corsica. The positive valued and rather short wavelength differences in the eastern end of line 2 and line 10 are due to real anomalies not mapped with their full amplitude in the altimetric gravity field. The 3.4 mgal mean difference between airborne and altimetric data seen in Table 3.5 is mainly due to the near-coastal problems; the mean difference for the open sea tracks is close to zero.

Table 3.5. Corsica data statistics and comparisons to some existing gravity models

Unit: mgal	Mean	Std. dev.	Minimum	Maximum
Airborne free air anomalies	-6.4	29.9	-78.3	91.3
Residuals relative to EGM96	-5.1	20.2	-72.8	47.2
Residuals relative to KMS01	-3.4	11.0	-52.6	39.2

The crossover statistics in Table 3.6 indicates a noise level of 2.6 mgal for the Great Barrier Reef and the Corsica survey and 3.0 mgal for the Crete survey. It is somewhat higher numbers than obtained in surveys performed with the Twin-Otter and the cause for that is likely to be the more long period phugoid motion of the Fokker as compared to the Twin-Otter. Even the data is noisier than those from the Greenland and the Baltic surveys they may still serve well for geoid computations. The noise has relatively little impact on the derived geoid, as long as it is short period leaving the medium to long wavelength components undisturbed.

Table 3.6. Crossover analysis

Data set	No of crossings	Max. Difference	RMS difference.
Great Barrier Reef	50	9.0 mgal	3.6 mgal
Crete	32	9.1 mgal	4.3 mgal
Corsica	25	7.2 mgal	3.7 mgal

Time constraints forced us to fly the Crete survey under weather conditions not optimal for airborne gravity. Wind driven turbulence over this mountainous island was at times quite severe preventing the acquisition of useful data. Also thermal driven turbulences can be an obstacle for airborne gravity over land areas. This was clearly demonstrated during some of the flights over the tropical Great Barrier Reef region. The Experience from both surveys was that flights over land should be done under good weather conditions, e.g. little wind when considering surveys over mountainous areas. Flying at night or early morning can minimize the impact of thermal driven atmospheric convection. Offshore flights, on the other hand, seem to be more insensitive to the weather conditions.

Conclusion

The KMS/UiB airborne gravity system based on a LaCoste & Romberg S-meter has proven to be a sturdy and reliable tool for airborne gravity operations under very diverse and often difficult operational conditions.

It was shown that cross correlation techniques offer a simple and reliable way to synchronize data from GPS with data from the gravimeter and from inertial measurement units. Such an approach simplifies the whole system concept, since there is no need for a common data logging and time tagging unit. The system is therefore flexible and easy to install in different aircraft. The most basic constellation consists of a GPS receiver, the gravimeter and a laptop.

Routines to identify and correct for some GPS related errors were outlined. Unfiltered gravity estimates showed to be a good indicator for artifact accelerations coming from GPS ambiguity fixing problems, especially under smooth flight conditions.

The concept of the apparent K-factor was introduced in order to access the combined response of GPS and the gravimeter to vertical accelerations. It was shown that this K-factor could not be considered a constant and an algorithm to determine a so-called filter-optimized K-factor was outlined. A modeling approach with a K-factor that varied as function of beam velocity was also tested, but it did not yield results that were convincingly better than the simpler filter-optimized K-factor approach.

The main contribution from this PhD work towards improved scalar gravimetry from stabilized platform systems is the new algorithm for tilt corrections, which ensures virtual unbiased results. That is a very important data property, especially when it comes to geodetic use of the data, but it also makes for more cost-effective and flexible use of the system. Since the data reduction scheme avoids the use of crossover adjustment of the survey lines, surveys can be done with much fewer crossing lines. The role of the crossing lines in surveys flown with our system is solely to get an internal noise estimate from the difference in the crossing points. Also single lines or coarse spaced lines obtained with our system may be utilized, e.g. to check marine surveys for long wavelength problems.

Comparisons to surface data yielded noise estimates consistent with those obtained from internal crossover analysis. The noise estimates ranged from 3.0 down to 2.6 mgal for the surveys flown with the Fokker F-27 and from 2.0 down to 1.3 mgal for the surveys flown with the Twin-Otter. The difference in quality of data obtained with the two aircraft is

ascribed to the fact that the Fokker, due to its size, exhibits more long period dynamics than the Twin-Otter. The data were routinely filtered to give a resolution of 6 km at a speed of 60 m/sec. It should be noticed that 6 km is a rather conservative estimate of the reachable resolution of the system. The filter can under low-turbulent conditions be shortened considerably and still yield virtual the same data accuracy.

Both GPS and gravimeter contribute to the total noise budget, but it seems like the gravimeter gives the main contribution. So there is still some room for gravity sensor improvements before GPS becomes the limiting factor. A hybrid system, where the vertical spring-type sensor is supplemented with a good accelerometer, could be a way to combine the superior long period performance of the LaCoste & Romberg gravimeter with the expected better high-dynamics characteristic of a good accelerometer.

Acknowledgement

The Danish Research Academy (Forskerakademiet) and National Survey and Cadastre - Denmark (KMS) provided the funding for my study including salary and travel support.
The research has been done within the frame of several projects initiated and headed by Rene Forsberg (the Skagerrak, the Greenland and the Baltic surveys), Bill Kearsley (the Great Barrier Reef survey) and Ilias Tziavos (the Crete and Corsica surveys). Funding for these projects came from European Union, National Imagery and Mapping Agency (NIMA) US, Australian Research Council, KMS, Norwegian Mapping Agency, Norwegian Petroleum Directorate, Norsk Hydro, Geodetic Survey of Sweden, Geodetic Survey of Finland and the Geological Survey of Sweden.
The author is thankful to my supervisors, Rene Forsberg (KMS) and Christian Tscherning (University of Copenhagen) for constructive advices and discussions during my work.
Airborne gravimetry is teamwork and I have been lucky to work together with a lot of dedicated and skillful people. First of all those of my colleagues from KMS, who took part in the airborne gravity campaigns: Rene Forsberg, Kristian Keller, Nynne Dalaa, Cecilia Nielsen and Sine Jacobsen. Also thanks to Arne Gidskehaug (University of Bergen) and Dag Solheim (Norwegian Mapping Agency) for good company during fieldwork and for fruitful discussions on the processing of airborne gravimetry.
Last but not least thanks to Bill Kearsley (University of New South Wales) for his hospitality and help during my stays in Sydney and thanks to the friends I got at UNSW.

References

Andersen, O. B., and P. Knudsen: The role of satellite altimetry in Gravity field modeling in Coastal areas, *Phys, chem. Earth (A),* **25**,1,17-24,2000

Andersen, O. B., P. Knudsen and R. Trimmer, The KMS99 global marine gravity field from ERS and GEOSAT satellite altimetry. Proceedings of the ERS/ENVISAT symposium. Looking down at the Earth in the new millenium, ESA publication office, Noordvijk, The Netherland, 2001.

Arabelos, D., R. Barzaghi, F. Sanso', G. Sona: The Gravimetric Geoid and the SST in the Eastern Mediterranean. Mare Nostrum, GEOMED Report no 4, Department of Geodesy and Surveying, University of Thessaloniki, 1994

Bastos, L., P. Tomé, T. Cunha, M. J. Fernandes and S. Cunha: Gravity Anomalies from Airborne Measurements-Experiments Using a Low Cost IMU Device. In: M. G. Siderius (ed.): Gravity, Geoid and Geodynamics 2000, IAG symposium Vol. 123, pp. 247-251, Springer Verlag, 2001

Brozena, J. M.: The Greenland Aerogeophysics Project: Airborne gravity, topographic and magnetic mapping of an entire continent. *In: From Mars to Greenland: Charting Gravity With Space and Airborne Instruments*. IAG symposium series 110, pp. 203-214, Springer Verlag, 1992.

Britting, K.R.: Inertial Navigation Systems Analysis. Wiley Interscience, Wiley & Sons, New York, 1971

Childers, V.A., D.C.McAdoo, J.M.Brozena and S.L.Laxon: New gravity data in the Arctic Ocean: Comparison of airborne and ERS gravity. *JGR,* **106**, B5, pp. 8871-8886, 2001.

Czompo, J.: *Airborne Scalar Gravimetry System Errors in the Spectral Domain*. Ph. D. Thesis, UCGE No 20067, Department of Geomatics Engineering, The University of Calgary, Canada, 1994.

Ferguson S.T. and Y. Hammada: Experiences with AIRGrav: Results from a New Airborne Gravimeter. In: M. G. Siderius (ed.): Gravity, Geoid and Geodynamics 2000, IAG symposium Vol. 123, pp. 211-216, Springer Verlag, 2001

Forsberg, R., K. Hehl, U. Meyer, A. Gidskehaug, L. Bastos: Development of an airborne geoid mapping system for coastal oceanography (AGMASCO). Proc. Int. Symp. of Gravity, Geoid and Marine Geodesy (GraGeoMar96), Tokyo, 1996.

Forsberg, R., A. V. Olesen and K. Keller: Airborne Gravity Survey of the North Greenland Shelf 1998. Kort - og Matrikelstyrelsen Technical Report no. 10, 1999.

Forsberg, R. and F. Rubek: *Gravity and GPS measurements in Greenland 1997*. Survey and data processing report, Office of Geodynamics, National Survey and Cadastre (KMS), Denmark, 1998.

Glennie, C.: An Analysis of Airborne Gravity by Strapdown INS/DGPS. Ph.D. Thesis, UCGE Report #20, Dept. of Geomatics Engineering, The University of Calgary, 1999

Glennie, C. and K. P. Schwartz: A comparison and analysis of airborne gravimetry results from two strapdown inertial DGPS systems. J. Geod. 73, pp 311-321, 1999

Gumert, W.R.: Airborne Gravity Measurements. In: *CRC Handbook of Geophysical Exploration at Sea*, Boca Raton Press, 1991.

Harlan, R. B.: Eotvos corrections for airborne gravimetry*, J. Geophys. Res.*, 3, 4675-4679, 1968.

Jekeli, C.: Inertial Navigation Systems with Geodetic Applications. Walter de Gruyter, Berlin, 2001

Kanasewich, E.R.: Time Sequence Analysis in Geophysics. The University of Alberta Press, 1975

Kwon, J. H. and C. Jekeli: A new approach for airborne vector gravimetry using GPS/INS. J. Geod 74, pp 690-700, 2001

LaCoste, L. B. J.: Measurement of Gravity at Sea and in the Air. *Reviews of Geophysics*, 5, 477-526, 1967.

LaCoste, 1973: Cross correlation method for evaluating and correction shipboard gravity data, Geophysics, 38, 701-709, 1973

LaFehr, T.R. and L.L Nettleton: Quantitative evaluation of a stabilized platform shipboard gravity meter, Geophysics, 32, 110-118, 1967.

Lemoine, F.G., S.C. Kenyon, J.K. Factor, R.G. Trimmer, N.K. Pavlis, D.S. Chinn, C.M. Cox, S.M. Klosko, S.B. Luthcke, M.H. Torrence,Y.M. Wang, R.G. Williamson, E.C. Pavlis, R.H. Rapp, and T.R. Olson: *The Development of the Joint NASA GSFC and the National Imagery and Mapping Agency (NIMA) Geopotential Model EGM96, NASA/TP-1998-206861*, Goddard Space Flight Center, Greenbelt, MD, July, 1998.

Moritz, H.: Geodetic Reference System 1980. Bulletin Géodésique, 66(2), 187-192, 1992

Olesen A V, R Forsberg, A Gidskehaug: *Airborne gravimetry using the LaCoste & Romberg gravimeter – an error analysis.* In: M.E. Cannon and G. Lechapelle (eds.). Proc. Int. Symp. on Kinematic Systems in Geodesy, Geomatics and Navigation, Banff, Canada, June 3-6, 1997, Publ.Univ. of Calgary, pp. 613-618, 1997.

Olesen, A.V., R. Forsberg and A. H. Kearsley: *Great Barrier Reef Airborne Gravity Survey (Braggs'99) - A Gravity Survey Piggybacked on an Airborne Bathymetry Mission*. In: M. G. Siderius (ed.): Gravity, Geoid and Geodynamics 2000, IAG symposium Vol. 123, pp. 247-251, Springer Verlag, 2001

Olesen, A.V., R. Forsberg, K. Keller, A. H. W. Kearsley: *Error sources in airborne gravimetry employing a spring-type gravimeter*. Proceedings from IAG 2001 Scientific Assembly, September 2-7, Budapest, Hungary. 2002a

Olesen, A.V., R. Forsberg and K. Keller: *Airborne Gravity Survey of Greenland's Continental Shelf*. Bulletin of the International Geoid Service, 2002b (accepted for publication)

Strykowski, G. and R. Forsberg: *Processing of marine gravity measurements off East Greenland: Contract report for NUNAOIL A/S*. Geodetic Division, National Survey and Cadastre of Denmark, 1995.

Swain C. J.: Horizontal acceleration corrections in airborne gravimetry. UCGE Special Report No 60010, Dept. of Geomatics Engineering, The University of Calgary, 1999

Schwarz, K.P.: Festschrift. Univ.Prof. em. Dr.-Ing. Wolfgang Torge sum 70. Geburtstag. University of Hannover, 2001

Thomson, L.G.D and L.J.B. LaCoste: Aerial Gravity Measurements. J. Geophys. Res., 65, 1, 305-322. 1960

Torge, W.: Gravimetry. Walter de Gruyter, Berlin, 1989

Valliant, H.: The LaCoste & Romberg air/sea gravimeter: an overview. In: *CRC Handbook of Geophysical Exploration at Sea*, Boca Raton Press, 1992.

Williams and MacQueen: Development of a versatile, commercially proven and cost-effective airborne gravity system. The Leading Edge, 2001

Appendix A. From raw GPS and gravimeter observations to filtered gravity estimates. A manual for the airborne gravity processing program AG.

The following is intended as a manual to the gravity processing program AG, developed by the author during my PhD project. A DOS/Windows version of the program and some sample data files can be downloaded from http://research.kms.dk/~avo/airgrav.html or with anonymous ftp from ftp.kms.dk/pub/avo/ag.zip. For a UNIX version contact Dag Solheim, Statens Kartverk, Norway, dag.solheim@statkart.no. You also need a postscript viewer like GSVIEW from Ghostgum Software Pty Ltd to access the graphical output from the program AG. The basic idea is that all processing parameters are determined through a visual analysis of the graphic processing output and iteratively entered into the processing via a text editor.
GPS processing is first briefly discussed but is not the main topic.

1 GPS processing.

The program GPSurvey from Trimble has become the de facto standard for kinematic GPS processing software here at KMS. Several other programs have been tested, but GPSurvey appears to yield the best results for airborne gravity, especially with noisy data. So-called ionosphere-free fixed-ambiguity type solutions are preferably used, but float type solutions are in some cases the only possibility. The processing strategy is fairly simple: do not include too many low elevation satellites, they will mainly add noise and make the ambiguity

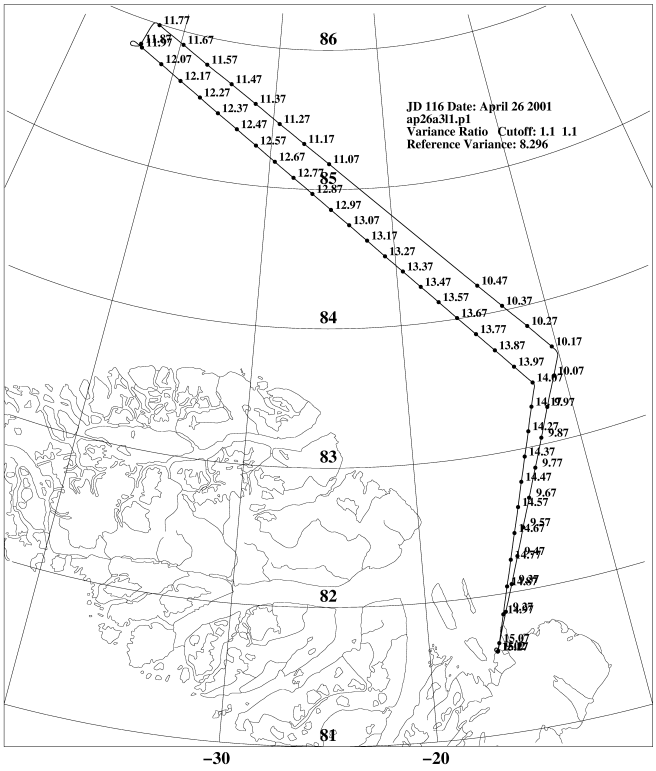

Figure 1. Ground track plot labeled with decimal hour. The flight is from the Greenland 2001 survey

fixing step more complicated. GPSurvey has several criteria for the quality of a given solution (reference variance, standard deviation, ratio test and pdop etc). Don't put too much significance to these criteria. Disable all masks (pdop-mask, ratio test and rms-mask etc), process more combinations of rover and reference receivers, and see which solution performs best in the gravity processing. A ground track plot labeled with time, like Figure 1, may facilitate the further gravity processing.

2 Gravity processing

The gravity processing is an iterative process. Changes to the processing parameters are entered with a text editor, the program AG is executed and the processing output, see Figure 2, is viewed with the postscript viewer. These three steps are repeated until no further improvements are obtained. All graphs mentioned in the sections below refer to Figure 2.

Line start and stop. Airborne gravity is processed on a line-by-line basis. The gravimeter beam is clamped during turns and the release of the beam marks the start of a new line. First the approximate time for line start and stop are extracted from a track plot like Figure 1. The exact start and stop time are determined from the raw gravity graph in the graphic output, see the middle panel in Figure 2. The raw gravity graph will exhibit extreme behavior if the beam is clamped and thus give a very accurate indication of when the beam was released at the start of the line and again clamped at the end of the line.

Synchronization. Next the synchronization graph in the upper panel is used to find the exact time shift between GPS data and gravimeter data. The time shift is changed iteratively until the correlation function peaks at zero time offset and the symmetry indicator is horizontal. The altimeter and INS data are synchronized the same way, if available.

Data gaps. Check the data gaps graph, a straight horizontal line if there is no data gaps. The GPS data has a gap around time 500 seconds in the example in Figure 2. The filtered gravity graph, lower panel black line, has a synchronous oscillation with a period close to the filter cut-off period. The oscillation is most likely induced by the data gap. Three different interpolation methods are implemented in the program, if none of them yields a reliable signal over the data gap then try another GPS solution. If worst comes to worst the filtered gravity data near the data gap has to be discarded.

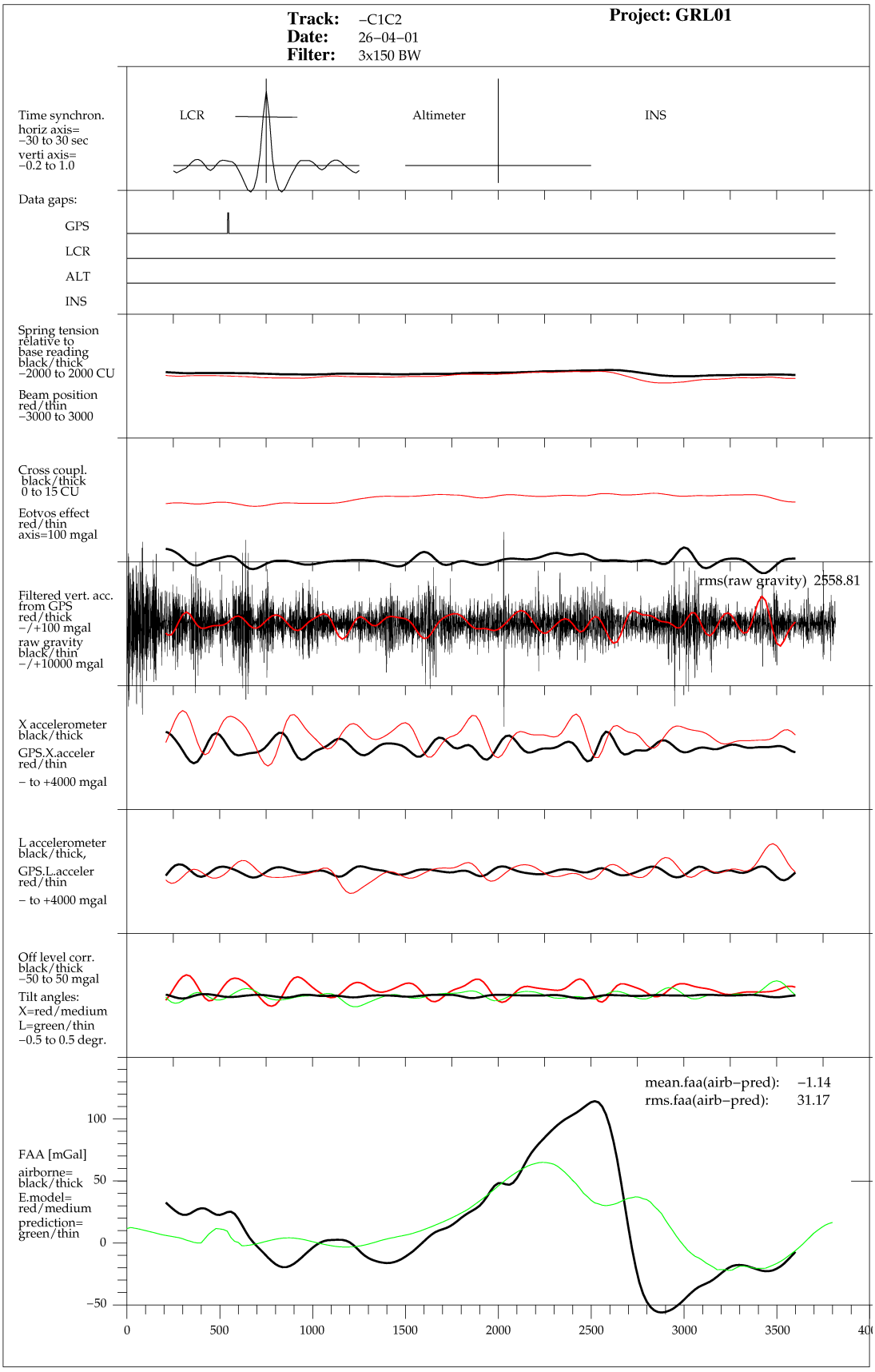

Figure 2. The postscript output

Filtered beam position. The spring tension is set before each line to equal the combined effect of expected gravity at altitude and Eötvös effect. If this presetting of the spring tension is to far from the actual values the beam may deviate from equilibrium (in average) and nonlinear effects may impact the data quality. As long as the filtered beam position graph stays within its panel it is considered safe.

Filtered cross coupling should not exceed –5 to +15 mgal. A combination of beam positions far from equilibrium (in average) and turbulent flight conditions may cause the cross coupling effect to become too severe to be modeled accurately enough.

The filtered vertical GPS acceleration graph should stay within its panel, otherwise nonlinear beam response effects are likely to impact the filtered gravity estimates. Any signal in the filtered gravity graph that correlates with the vertical acceleration graph is a danger signal. Check whether the right K-factor model is used? If yes, then the only thing to do is to increase the filter length or discard the data.

Raw gravity is a good indicator of the flight conditions. An RMS value of appr. 2500 mgal, as in Figure 2, indicates a smooth flight. Sudden peak values of magnitude close to a multiple of 20000 mgal indicate an ambiguity fixing problem in the GPS solution. The synchronous oscillation with a period close to the filter cut-off period in the filtered gravity graph confirms this. Run AG with the CS parameter set to 1. Edit the file 'raw.g' as shown in Figure 2.10 in section 2.7, and rerun AG with the CS parameter set to 2.

Filtered vertical acceleration difference graph can be activated instead of raw gravity graph. It will show the difference between GPS and altimeter derived accelerations. The signal should be small for offshore flights. The graph is not activated in the example shown in Figure 2.

Filtered X- and L-accelerations will normally stay well within the panel. Changes in heading or speed can cause large values and thereby induce a severe tilting of the platform. If so check the off-level correction graph.

The filtered off-level correction graph should be compared closely with the filtered gravity graph. If there is some degree of correlation between the two signals it could indicate that,

the off-level correction is degraded. Check whether the calibration factors for the horizontal accelerometers are correct.

The surface data graph should closely resemble the filtered airborne gravity data in areas with good surface data coverage. That is only the case around 3500 seconds in Figure 2.

3 Flowchart

Figure 3 gives the overall picture off the processing data flow. Some of the tests described above are shown as well. The detailed equations used in each processing step can be found in chapter 1 or 2 or in the program code available at ftp.kms.dk/pub/avo/ag.zip.

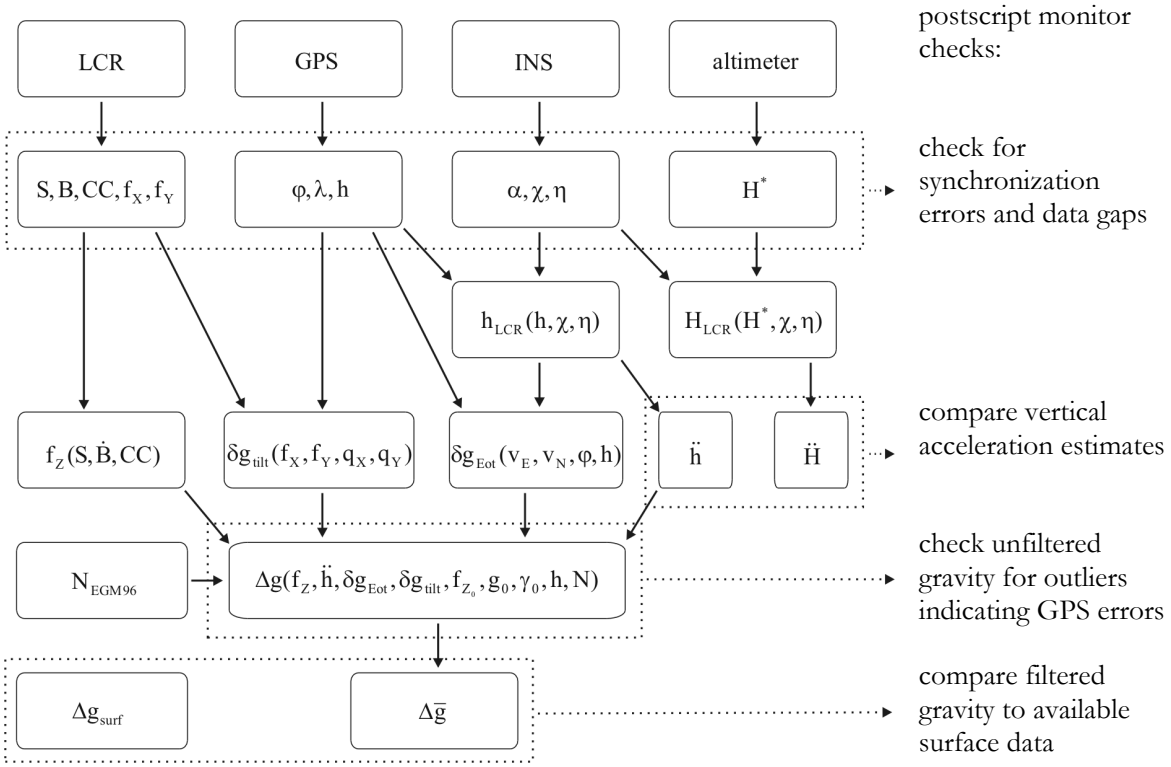

Figure 3. Processing flowchart

Notation:

LCR	LaCoste & Romberg air/sea gravimeter
GPS	Global Positioning System
INS	Inertial Navigation System
altimeter	laser or radar altimeter

see also next page

S, B, CC, f_X, f_Y	spring tension, beam position, cross coupling, cross and long horizontal accelerometer output
φ, λ, h	latitude, longitude and ellipsoidal height
α, χ, η	aircraft attitude angles: yaw, pitch and roll
H^*	altimeter reading
h_{LCR}	height of gravimeter above ellipsoide
H_{LCR}	do above sea surface
f_Z	computed vertical gravimeter output
δg_{tilt}	platform off-level effect
q_X, q_Y	kinematic horizontal accelerations derived from GPS positions
δg_{Eot}	Eötvös effect
$v_{E,}, v_N$	eastern and northern velocity from GPS positions
$\ddot{h}, \ddot{H}$	vertical accelerations from GPS and altimeter
N_{EGM96}	geoid model
Δg	unfiltered airborne gravity anomaly
f_{Z_0}, g_0	airport base reading and corresponding gravity value
Δg_{surf}	gravity anomaly from surface data
$\Delta \bar{g}$	filtered airborne gravity anomaly

Appendix B. Papers appended to the original Ph.D. thesis.

B1 Olesen A V, R Forsberg, A Gidskehaug: *Airborne gravimetry using the LaCoste & Romberg gravimeter – an error analysis.* In: M.E. Cannon and G. Lechapelle (eds.). Proc. Int. Symp. on Kinematic Systems in Geodesy, Geomatics and Navigation, Banff, Canada, June 3-6, 1997, Publ.Univ. of Calgary, pp. 613-618, 1997.

B2 Olesen, A. V., R. Forsberg, K. Keller and A. Gidskehaug: *Airborne gravity survey of the Polar Sea north of Greenland.* In: Proc. EAGE 61st Conference, Helsinki, extended abstract 2-37 (4 pp.), 1999.

B3 Olesen, A. V.,R. Forsberg, K. Keller, A. Gidskehaug: *Airborne Gravity Survey of Lincoln Sea and Wandel Sea, North Greenland.* Chemistry and Physics of the Earth, Vol 25 A, pp. 25-29, 2000.

B4 Olesen, A.V., R. Forsberg and A. H. Kearsley: *Great Barrier Reef Airborne Gravity Survey (Braggs'99) - A Gravity Survey Piggybacked on an Airborne Bathymetry Mission*. In: M. G. Siderius (ed.): Gravity, Geoid and Geodynamics 2000, IAG symposium Vol. 123, pp. 247-251, Springer Verlag, 2001

B5 Olesen, A.V., R. Forsberg, K. Keller, A. H. W. Kearsley: *Error sources in airborne gravimetry employing a spring-type gravimeter*. In: J. Ádám and K.P. Schwarz (eds.): Vistas for Geodesy in the New Millennium, IAG symposiom Vol. 125, pp 205-210, Springer Verlag, 2002

B6 Olesen, A.V., R. Forsberg and K. Keller: *Airborne Gravity Survey of Greenland's Continental Shelf*. Bulletin of the International Geoid Service, 2002 (accepted for publication) 11 pp

B7 Olesen, A.V., O.B. Andersen and C.C Tscherning: Merging of airborne gravity and gravity derived from satellite altimetry: test cases along the coast of Greenland. Studia geophysica et geodaetica, 2002 (in press) 8 pp

National Survey and Cadastre – Denmark (KMS), Technical Reports

The National Survey and Cadastre – Denmark, Technical Report series is intended as an informal report series, published at irregular intervals. The following reports have so far been published in the series (up to number 3, the reports were named "Geodætisk Institut, Technical Reports", from number 4 through 7, the reports were named "National Survey and Cadastre – Denmark, Geodetic Division, Technical Reports").

1. Jørgen Eeg: *On the Adjustment of Observations in the Presence of Blunders*, 32 pp., 1986.
2. Per Knudsen, C.C. Tscherning and René Forsberg: *Gravity Field Mapping Around the Faeroe Islands and Rockall Bank from Satellite Altimetry and Gravimetry*, 30 pp., 1987.
3. Niels Andersen: *The Structure and Filling of a 19.2 Kilometer Hydrostatic Leveling Tube*, 83 pp., 1988.
4. René Forsberg: *Gravity Measurements in East Greenland 1986-1988*, 32 pp., 1991.
5. Gabriel Strykowski: *Automation Strategy for Repeated Tasks in DOS*, 15 pp., 1992.
6. Simon Ekholm and Kristian Keller: *Gravity and GPS Survey on the Summit of the Greenland Ice Sheet 1991-1992*, 26 pp., 1993.
7. Per Knudsen: *Integrated Inversion of Gravity Data*, 52 pp., 1993.
8. Thomas Knudsen: *Geophysical Use of Geographical Information Systems*, 76 pp., 1996.
9. Simon Ekholm: *Determination of Greenland Surface Topography from Satellite Altimetry and Other Elevation Data*, 23 pp., 1997.
10. René Forsberg, Arne Olesen and Kristian Keller: *Airborne Gravity Survey of the North Greenland Shelf 1998*, 34 pp., 1999.
11. Cecilia S. Nielsen: *Topography and Surface Velocities of an Irregular Ice Cap in Greenland Assessed by the means of GPS, Laser Altimetry and SAR Interferometry*, 81 pp., 2001.
12. Cecilia S. Nielsen: *Estimation of Ice Topography and Surface Velocities Using SAR Interferometry*, 37 pp., 2001
13. Thomas Knudsen (ed): *Proceedings of the seminar on remote sensing and image analysis techniques for revision of topographic databases, Copenhagen, Denmark 2000-02-29*, 119 pp., 2000.
14. Lars Brodersen: *Maps as Communication - Theory and Methodology in Cartography*, 88 pp., 2001.
15. Claus V. Petersen og Simon Ekholm: *Analyse af digitale terrænmodeller beregnet fra satellitbåren SAR interferometrii, Case studies af udvalgte områder i Grønland og Danmark,* 20 pp., 2001.
16. Olwijn Leeuwenburgh: *Combined Analysis of Sea Surface Height and Temperature for Mapping and Climate Studies*, 96 pp., 2001.
17. Călin Arens: *Some examples of topographic applications and accuracy of laser scanning.* 66 pp, 2002.
18. Rene Forsberg, Arne V. Olesen, Kristian Keller and Mads Møller: *Airborne Gravity Survey of Sea Areas Around Greenland and Svalbard 1999-2001,* 55 pp., 2002.
19. Jacob L. Høyer: *On the combination of satellite and in situ observations to detect oceanic processes*, 116 pp, 2002.
20. Thomas Knudsen: *"True" colour presentation of suburban areas from colour-infrared aerial photos*, 51 pp, 2001.
21. R. Forsberg, K. Keller, S. M. Hvidegård and A. Olesen: *ESAG-2002: European airborne gravity and lidar survey in the Arctic Ocean,* 28 pp., 2002.
22. R. Forsberg, A. Olesen: *Airborne gravity survey of the Foxe Basin, Nunavut,* 13 pp., 2002.
23. P. Knudsen, O.B. Andersen, T. Knudsen, O. Leeuwenburgh, J. L. Høyer, A. A.Nielsen, K. B. Hilger,

C. C. Tscherning, N. K. Højerslev, G. Moreaux, E. Buch og V. Huess *Geoid and Sea Level of the North Atlantic Region – GEOSONAR – Final Report*, 40 pp, 2003.

24. A. V. Olesen: *Improved airborne scalar gravimetry for regional gravity field mapping and geoid determination,* 55 pp, 2003.

Reports may be ordered from the individual authors at the following address: Kort & Matrikelstyrelsen, Rentemestervej 8, DK-2400 Copenhagen NV, Denmark, Internet: www.kms.dk